

UT-14-29
June, 2014

Studying Inflation with Future Space-Based Gravitational Wave Detectors

Ryusuke Jinno^(a), Takeo Moroi^(a) and Tomo Takahashi^(b)

^(a)*Department of Physics, The University of Tokyo, Tokyo 113-0033, Japan*

^(b)*Department of Physics, Saga University, Saga 840-8502, Japan*

Abstract

Motivated by recent progress in our understanding of the B -mode polarization of cosmic microwave background (CMB), which provides important information about the inflationary gravitational waves (IGWs), we study the possibility to acquire information about the early universe using future space-based gravitational wave (GW) detectors. We perform a detailed statistical analysis to estimate how well we can determine the reheating temperature after inflation as well as the amplitude, the tensor spectral index, and the running of the inflationary gravitational waves. We discuss how the accuracies depend on noise parameters of the detector and the minimum frequency available in the analysis. Implication of such a study on the test of inflation models is also discussed.

1 Introduction

The B -mode signal in the cosmic microwave background (CMB) provides important information about the primordial inflation responsible for the generation of the cosmic density fluctuations. In particular, since the gravitational waves (GWs) produced during inflation is likely to be the origin of the B -mode signal, the amplitude of the inflationary gravitational waves (IGWs), at least for the scale relevant for the CMB, will be understood once the B -mode signal is observed. Recently the discovery of the B -mode signal has been announced by BICEP2 [1] and the reported tensor-to-scalar ratio is relatively large (i.e., $r_{\text{BICEP2}} = 0.20^{+0.07}_{-0.05}$): such a value of the tensor-to-scalar ratio is consistent with the prediction of so-called large-field inflation like chaotic inflation [2]. However, after the announcement of the BICEP2 result, it was pointed out that the BICEP2 signal may be significantly affected by the polarized dust emission [12, 13]. Even in such a case, some fraction of the signal could originate from IGWs and hence a relatively large IGW amplitude may still be allowed. The large value of the tensor-to-scalar ratio opens up a new possibility to detect and study the properties of the IGWs by direct detection experiments in the future [3–10]. Therefore, it would be interesting to consider to what extent we can obtain the information on the inflationary dynamics from future direct-detection experiments of GWs.^{#1}

Importantly, the information about the dynamics of inflation is imprinted in the IGWs. In particular, the spectral index and the running of the IGW spectrum depend on how the inflaton evolves during inflation. This fact implies that the determination of these parameters from the IGWs may enable us to acquire the information about the shape of the inflaton potential [14]. Furthermore, the IGW spectrum is also sensitive to the history of the universe so that the information about the cosmic expansion is embedded in it. In particular, the IGW spectrum changes its behavior at the frequency corresponding to the time of the reheating due to the inflaton decay [15].^{#2} If the spectrum of the IGWs is precisely studied, we may acquire information about the very early epoch of the universe.

The possibilities of detecting and studying the IGWs with future space-based GW detectors, like Big Bang Observer (BBO) [22] and DECi-hertz Interferometer Gravitational wave Observatory (DECIGO) [23], have been intensively studied. In particular, some of these detectors are expected to detect the IGW signal if $r \sim 0.1$ which is predicted by the chaotic inflation (and also if there is no significant suppression of the IGW amplitude at the frequency range of ~ 1 Hz compared to that at the CMB scale). In fact, the sensitivities of these detectors are planned to be so high that they may not only detect the IGWs but also study their properties. Notably, these space-based GW detectors are sensitive to the GWs at the frequency of $\sim 0.1 - 10$ Hz, which enters the horizon when the cosmic temperature is about $10^7 - 10^9$ GeV. Thus, we may have a chance to learn what happened in the universe at such a high temperature with those GW detectors. Since there will be more data coming on the B -mode polarization of CMB in the near future from Planck and other experiments, it would be now worth revisiting the question of what kind of information we may acquire

^{#1} For future prospects of probing gravitational waves using B -mode in light of the BICEP2 result, see [11].

^{#2} For the works studying the thermal history with GWs along this line, see [16–21].

with the future space-based GW detectors.

In this paper, we investigate how and how well we can study the properties of the IGWs with future GW experiments. For this purpose, assuming future space-based GW experiments, we calculate the signal-to-noise ratio for given fiducial models. The size of the signal is assumed to be the one predicted in the chaotic inflation, while the noise functions are estimated for several choices of detector parameters. We first consider the measurements of IGW parameters for the case where the reheating temperature is so high that the IGW spectrum in the sensitivity range of the GW detectors is insensitive to T_R . We study how well we can measure the amplitude, the spectral index, and its running. Then, we discuss the case where T_R is relatively low.

The organization of this paper is as follows. In Section 2, we briefly review basic properties of the IGW. The statistical method we adopt in this paper is summarized in Section 3. The numerical results are shown in Section 4. In Section 5, we discuss the implication of the study of the IGW spectrum on the test of inflation models. In particular, we discuss how the prediction of the chaotic inflation model can be tested. Section 6 is devoted for conclusions and discussion.

2 IGW Spectrum

We first briefly review basic properties of the IGWs for the case where there is no entropy production after the decay of inflaton. For our analysis, it is convenient to define the present GW energy density per log frequency normalized by the critical density ρ_{crit} :

$$\Omega_{\text{IGW}}(f) \equiv \frac{1}{\rho_{\text{crit}}} \frac{d\rho_{\text{IGW}}}{d \ln f}, \quad (2.1)$$

where f is the frequency of the GWs and ρ_{IGW} is the total energy density of the IGW integrated over frequency.

The IGW spectrum Ω_{IGW} strongly depends on the reheating temperature after inflation. In our analysis, we evaluate the reheating temperature as^{#3}

$$T_R \equiv \left(10 \frac{\Gamma_\phi^2 M_{\text{Pl}}^2}{g(T_R) \pi^2} \right)^{1/4}, \quad (2.2)$$

with Γ_ϕ being the decay rate of the inflaton and $M_{\text{Pl}} \simeq 2.4 \times 10^{18}$ GeV being the reduced Planck mass. In addition, $g(T)$ is the effective number of massless degrees of freedom at the temperature of T ; we use the standard-model prediction of $g(T \gg 100 \text{ GeV}) = 106.75$, and

^{#3}Here, we assume the perturbative decay of the inflaton in the reheating process. If the parametric resonance occurs, Eq. (2.2) is modified; in such a case, the reheating temperature is given by $T_R \sim \sqrt{\Gamma_\phi^{(\text{P.R.})}} M_{\text{Pl}}$, where $\Gamma_\phi^{(\text{P.R.})}$ is the particle-production rate due to the parametric resonance at the end of the reheating process. Since the effect of the parametric resonance is model-dependent, hereafter, we consider the case where reheating process proceeds via the perturbative decay of the inflaton.

$g(T_{\text{eq}}) = 3.36$ (with T_{eq} being the temperature at the time of radiation-matter equality). We denote the frequency of the mode entering the horizon at the time of the reheating as f_{R} , which is approximately given by

$$f_{\text{R}} \simeq 0.3 \text{ Hz} \times \left(\frac{T_{\text{R}}}{10^7 \text{ GeV}} \right). \quad (2.3)$$

In the frequency range of our interest, Ω_{IGW} is given by the following form:

$$\Omega_{\text{IGW}}(f) = \bar{\Omega}_{\text{IGW}}(f) \mathcal{T}(f), \quad (2.4)$$

where the function $\mathcal{T}(f)$ contains information about the reheating temperature; $\mathcal{T}(f) \rightarrow 1$ as $f \ll f_{\text{R}}$.

We parameterize the primordial spectrum $\bar{\Omega}_{\text{IGW}}$ by introducing the amplitude, the tensor spectral index, and its running, which are defined as

$$n_{\text{T}}(f_*) \equiv \left[\frac{d \ln \bar{\Omega}_{\text{IGW}}(f)}{d \ln f} \right]_{f=f_*}, \quad \alpha_{\text{T}}(f_*) \equiv \left[\frac{d^2 \ln \bar{\Omega}_{\text{IGW}}(f)}{d(\ln f)^2} \right]_{f=f_*}, \quad (2.5)$$

with f_* being the pivot scale. In slow-roll inflation models, the parameters n_{T} and α_{T} are expected to be much smaller than 1. We will discuss how well we can constrain these parameters with future space-based GW detectors. It should be noted that, because $\Omega_{\text{IGW}}(f)$ does not depend on the pivot scale, the following relations hold:

$$\ln \bar{\Omega}_{\text{IGW}}(f') = \ln \bar{\Omega}_{\text{IGW}}(f_*) + n_{\text{T}}(f_*) \ln(f'/f_*) + \frac{1}{2} \alpha_{\text{T}}(f_*) \ln^2(f'/f_*), \quad (2.6)$$

$$n_{\text{T}}(f'_*) = n_{\text{T}}(f_*) + \alpha_{\text{T}}(f_*) \ln(f'_*/f_*), \quad (2.7)$$

where we neglect the contributions of higher-order expansion parameters. Thus, the error in one parameter contaminates into those of other parameters if we change the pivot scale. In other words, with a proper choice of f_* , the error of $\bar{\Omega}_{\text{IGW}}(f_*)$ (or $n_{\text{T}}(f_*)$) can be minimized. We will see that this happens when f_* is chosen to be the frequency at which the GW detector has the best sensitivity. We also note here that, if we limit ourselves to second order in the expansion with respect to $\ln(f/f_*)$, $\bar{\Omega}_{\text{IGW}}$ is given in the following form:

$$\bar{\Omega}_{\text{IGW}}(f) \simeq \bar{\Omega}_{\text{IGW}}(f_*) \left(\frac{f}{f_*} \right)^{n_{\text{T}}(f_*) + \frac{1}{2} \alpha_{\text{T}}(f_*) \ln(f/f_*)}. \quad (2.8)$$

As we have mentioned, the effect of the reheating is embedded in the function \mathcal{T} . We can understand the qualitative behavior of \mathcal{T} by using the fact that the amplitude of the IGW is almost constant when the wavelength is longer than the horizon scale while it decreases as a^{-2} (with a being the scale factor) once it enters the horizon. For $f \gg f_{\text{R}}$, $\mathcal{T} \propto f^{-2}$. On the contrary, for $f \ll f_{\text{R}}$, \mathcal{T} becomes close to 1. If the reheating temperature is not high enough, a slight deviation from the relation $\mathcal{T} = 1$ may affect the determination of the

IGW parameters n_T , and α_T . When the universe is dominated by the inflaton oscillation, the IGW amplitude behaves as $\sim j_1(k\tau)/k\tau$, where j_1 is the spherical Bessel function, k is the conformal wavenumber, and τ is the conformal time. Then, for $k\tau \ll 1$, which holds for superhorizon modes, the evolution of the IGW amplitude has a slight dependence on k as $\sim 1 + (k\tau)^2/10$, which results in a slight deviation from $\mathcal{T} = 1$. For the mode with $f \ll f_R$, we expect $\mathcal{T}(f) \simeq 1 + c(f/f_R)^2$, with c being a numerical constant. We have numerically calculated c , and found $c \simeq -0.3$. Thus, if f is one or two orders of magnitude smaller than f_R , the small correction to \mathcal{T} has minor effects on the measurements of n_T and α_T as far as they are of the order of $10^{-2} - 10^{-3}$. For the IGW spectrum of $f \sim 1$ Hz, this is the case when the reheating temperature is higher than $\sim 10^8 - 10^9$ GeV. Because the effect of the reheating becomes negligible when f_R is order of magnitude larger than the frequency range relevant for the GW detectors, two types of analyses are suggested. One is the analysis with the assumption of high enough reheating temperature; then we may impose $\mathcal{T} = 1$ and determine $\bar{\Omega}_{\text{IGW}}$, n_T , and α_T . The other is the one with T_R being included. Then, we may have information about the reheating temperature. In Section 4, we consider both cases.

In our analysis, \mathcal{T} is evaluated by numerically solving the evolution equation of GWs. In Fig. 1, we show the spectrum of the IGWs for several choices of parameters. One can see a significant suppression of Ω_{IGW} in the high frequency region.

With the inflation model being fixed, Ω_{IGW} can be evaluated. In single-field slow-roll inflation model, $\bar{\Omega}_{\text{IGW}}$ is given by

$$\bar{\Omega}_{\text{IGW}}(f_*) = \frac{1}{3} \Omega_{\text{rad}} \left(\frac{H_*}{2\pi M_{\text{Pl}}} \right)^2 \left(\frac{g(T_{f_*})}{g(T_{\text{eq}})} \right) \left(\frac{g_s(T_{f_*})}{g_s(T_{\text{eq}})} \right)^{-4/3}, \quad (2.9)$$

where $\Omega_{\text{rad}} \simeq 9.4 \times 10^{-5}$ is the density parameter of radiation component, H_* is the expansion rate of the universe when the mode f_* exits the horizon during inflation, and $g_s(T)$ is the effective number of massless degrees of freedom for entropy density at the temperature T . (Here and hereafter, the subscript “*” is used for quantities related to the mode with $f = f_*$.) In addition, $T_{f_*} \gg 100$ GeV is the temperature at the time of the horizon reentry of the mode f_* . In the standard model, $g_s(T \gg 100 \text{ GeV}) = 106.75$, and $g_s(T_{\text{eq}}) = 3.91$.

The tensor spectral index n_T and its running α_T are related to the so-called slow-roll parameters as

$$n_T(f_*) = -2\epsilon_*, \quad (2.10)$$

$$\alpha_T(f_*) = -2\epsilon_* (4\epsilon_* - 2\eta_*), \quad (2.11)$$

where the quantities in the right-hand sides should be evaluated when the mode with $f = f_*$ exits the horizon, and

$$\epsilon = \frac{1}{2} M_{\text{Pl}}^2 \left(\frac{V'}{V} \right)^2, \quad \eta = M_{\text{Pl}}^2 \left(\frac{V''}{V} \right). \quad (2.12)$$

Here V is the potential of inflaton, with the “prime” being the derivative with respect to the inflaton field. We also note here that the amplitude of the scalar-mode fluctuations is

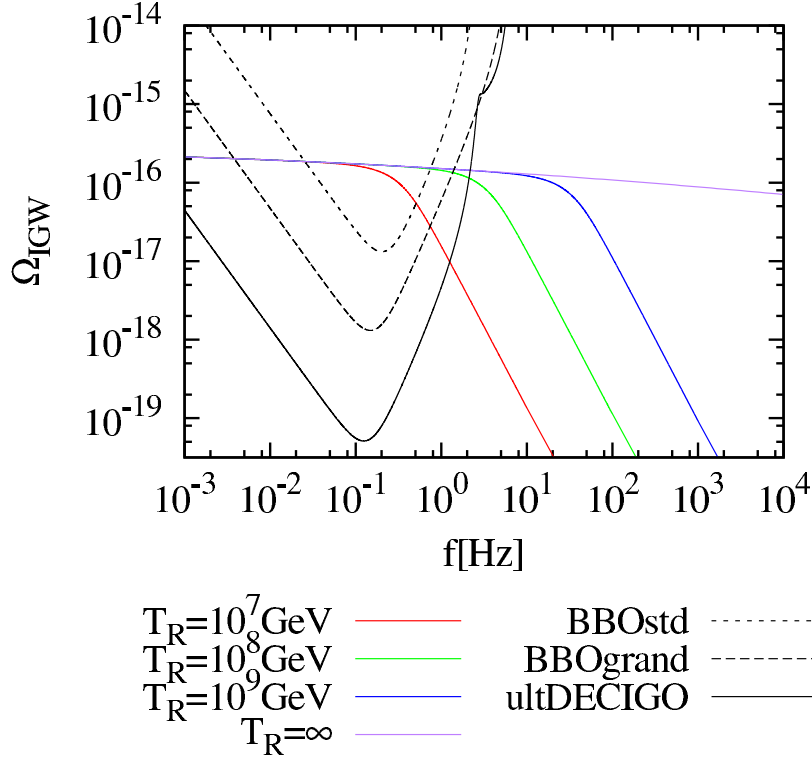


Figure 1: Spectrum of the IGWs as a function of the frequency. Here, we take $\bar{\Omega}_{\text{IGW}} = 1.51 \times 10^{-16}$, $n_T = -6.38 \times 10^{-2}$, and $\alpha_T = -4.08 \times 10^{-3}$. The reheating temperature is taken to be $T_R = 10^7$ GeV (red), $T_R = 10^8$ GeV (green), $T_R = 10^9$ GeV (blue), and high enough T_R (purple). The black lines are the effective sensitivity to the GW amplitude defined in Eq. (3.21).

obtained as

$$A_S = \frac{1}{2\epsilon} \left(\frac{H}{2\pi M_{\text{Pl}}} \right)^2. \quad (2.13)$$

The purpose of the present study is to analyze the accuracy of the determinations of $\bar{\Omega}_{\text{IGW}}$, n_T , α_T , and T_R in future space-based GW detectors. The accuracy, however, depend on the underlying (fiducial) values of these parameters. Here, we take the chaotic inflation model with a quadratic potential [2] as an example and evaluate the quantities introduced above. (This model predicts the tensor-to-scalar ratio of $r \simeq 0.15$, which is consistent with the BICEP2 observation.) We adopt the inflaton potential of the following form

$$V = \frac{1}{2} m_\phi^2 \phi^2. \quad (2.14)$$

With the above inflaton potential, inflation occurs if the inflaton ϕ starts its motion with the initial amplitude much larger than the reduced Planck scale. The evolution of the inflaton,

T_R	$\bar{\Omega}_{\text{IGW}}(1 \text{ Hz})$	$n_T(1 \text{ Hz})$	$\alpha_T(1 \text{ Hz})$
10^7 GeV	1.41×10^{-16}	-0.0751	-0.00564
10^8 GeV	1.44×10^{-16}	-0.0710	-0.00504
10^9 GeV	1.48×10^{-16}	-0.0672	-0.00451
10^{10} GeV	1.51×10^{-16}	-0.0639	-0.00408
10^{11} GeV	1.54×10^{-16}	-0.0609	-0.00370
10^{12} GeV	1.57×10^{-16}	-0.0581	-0.00337

Table 1: The values of $\bar{\Omega}_{\text{IGW}}$, n_T , and α_T at 1 Hz in the chaotic inflation model for several values of the reheating temperature.

as well as that of the energy density of radiation, are governed by the following equations:

$$\ddot{\phi} + 3H\dot{\phi} + m_\phi^2\phi = -\Gamma_\phi\dot{\phi}, \quad (2.15)$$

$$\dot{\rho}_{\text{rad}} + 4H\rho_{\text{rad}} = \Gamma_\phi\dot{\phi}^2, \quad (2.16)$$

where the “dot” denotes the derivative with respect to time, ρ_{rad} is the energy density of radiation and Γ_ϕ is the decay rate of the inflaton. We follow the evolution of the universe by numerically solving the above equations. Then, we calculate $\bar{\Omega}_{\text{IGW}}$ by using Eq. (2.9). The value of $\bar{\Omega}_{\text{IGW}}$, as well as A_S , depend on the inflaton mass m_ϕ and the reheating temperature T_R . Here, we fix m_ϕ by requiring the amplitude for the scalar fluctuations A_S to satisfy [24]:

$$A_S(0.05 \text{ Mpc}^{-1}) = 2.215 \times 10^{-9}. \quad (2.17)$$

For the reheating temperature of $T_R = 10^{7-12} \text{ GeV}$, the best-fit value of m_ϕ is given by $(1.6 - 1.7) \times 10^{13} \text{ GeV}$. In Table 1, we show the values of $\bar{\Omega}_{\text{IGW}}$, n_T , and α_T for several values of the reheating temperature. We also note here that, if the inflaton interacts with the standard-model particles with dimension-5 operator suppressed by the Planck scale, the decay rate of the inflaton is roughly estimated to be

$$\Gamma_\phi \sim \frac{1}{4\pi} \frac{m_\phi^3}{M_{\text{Pl}}^2}. \quad (2.18)$$

(Such a Planck suppressed interaction may arise if the cut-off scale of the standard model is around the Planck scale.) Taking $m_\phi \sim 10^{13} \text{ GeV}$, such a value of the decay rate results in the reheating temperature of $\sim 10^{10} \text{ GeV}$.

Before closing this section, we comment on our treatment of n_T . In the slow-roll single-field inflation model, the tensor spectral index n_T is related to the tensor-to-scalar ratio r if these parameters are defined at the same wave-length (or frequency). They are related as $n_T = -\frac{1}{8}r$ at the leading order of the slow-roll parameters. However, this relation hardly helps to fix $n_T(f_*)$; experimental determination of the tensor-to-scalar ratio at f_* is difficult since the information on the scalar-mode fluctuations at such a small scale will not be

available. In addition, the value of r at $f \sim f_*$ and that at the CMB scale (i.e., $\sim 0.05 \text{ Mpc}^{-1}$) are model-dependent and may significantly deviate. For example, in the chaotic inflation model, $r(0.05 \text{ Mpc}^{-1})/r(k_*) \sim 3$. Thus, we treat $n_T(f_*)$ as one of the parameters which should be determined.

3 Statistical Analysis

Now we summarize how we estimate the underlying parameters which govern the shape of the IGWs. In the situation of our interest, the data from the GW detector have information about the IGWs, while they are also affected by the noise. To reduce the effect of the noise, the GW detectors with time-delay interferometry (TDI) method may be used, which we assume in our analysis. In particular, we concentrate on two sets of spacecrafts at the vertices of (nearly) regular triangles. The first and second sets provide the TDI variables so-called (A, E, T) and (A', E', T') , respectively, which are linear combinations of the fluctuations of the laser frequency, normalized by the center one, measured at each spacecraft. Written explicitly, each data stream $s_I(f)$ is

$$s_A = \frac{1}{\sqrt{2}}(\alpha - \gamma), \quad (3.1)$$

$$s_E = \frac{1}{\sqrt{6}}(\alpha - 2\beta + \gamma), \quad (3.2)$$

$$s_T = \frac{1}{\sqrt{3}}(\alpha + \beta + \gamma). \quad (3.3)$$

Here

$$\alpha = y_{21}(t) - y_{31}(t) + y_{13}(t - L_2) - y_{12}(t - L_3) + y_{32}(t - L_1 - L_2) - y_{23}(t - L_1 - L_3), \quad (3.4)$$

with y_{ij} being the normalized fluctuation of the laser frequency, propagating along arm i (the one opposite to the spacecraft i) and measured by spacecraft j [14, 25, 26]. In addition, β and γ are obtained by the cyclic permutations of the indices as $1 \rightarrow 2 \rightarrow 3 \rightarrow 1$. The important point is that the noises of the variables A, E, T (and those of A', E', T') are uncorrelated. Thus, with those variables, a high signal-to-noise ratio may be realized. Each data stream is given by the sum of the GW signal H_I and the noise n_I :

$$s_I(f) = H_I(f) + n_I(f). \quad (3.5)$$

The signal is linear in the amplitude of the IGWs. We expand the fluctuation of the metric for the tensor mode, $h_{ij} = g_{ij} - \delta_{ij}$, as

$$h_{ij} = \sum_{P=+, \times} \int_{-\infty}^{\infty} df \int d\hat{n} h_P(f, \hat{n}) e^{2\pi i f(t - \hat{n}\vec{x})} \epsilon_{ij}^P(\hat{n}), \quad (3.6)$$

where ϵ_{ij}^P is the polarization tensor (whose normalization is $\epsilon_{ij}^P \epsilon_{ij}^{P'} = 2\delta_{PP'}$), and \hat{n} is the unit vector pointing to the direction of the propagation. In the present convention,

$$\langle h_P^*(f, \hat{n}) h_{P'}(f, \hat{n}) \rangle = \frac{1}{8\pi} \delta(f - f') \delta(\hat{n} - \hat{n}') \delta_{PP'} S_h(f, \hat{n}), \quad (3.7)$$

where $\langle \dots \rangle$ denotes the ensemble average and

$$S_h(f) = \frac{3H_0^2}{4\pi^2} f^{-3} \Omega_{\text{IGW}}(f), \quad (3.8)$$

with H_0 being the present Hubble parameter.

Because the IGW amplitude is so small that the signal can be well approximated to be proportional to h_P , the GW signal can be expressed in the following form:

$$H_I(f) = \sum_{P=+, \times} \int d\hat{n} R_I(f, \hat{n}, P) h_P(f, \hat{n}). \quad (3.9)$$

Here, the information about the detector geometry is embedded into the function R_I [27], with which the overlap reduction function can be obtained (see Eq. (3.11) below). Then, the two-point correlator of the signal becomes

$$\langle H_I^*(f) H_J(f') \rangle = \frac{\gamma_{IJ}}{5} \delta(f - f') S_h(f), \quad (3.10)$$

where the overlap reduction function is given by

$$\gamma_{IJ} \equiv \frac{5}{2} \sum_{P=+, \times} \int \frac{d\hat{n}}{4\pi} R_I^*(f, \hat{n}, P) R_J(f, \hat{n}, P). \quad (3.11)$$

In Fig. 2, we plot γ_{IJ} for several choices of (I, J) .^{#4}

For the calculation of the data stream given in Eq. (3.5), the noise power spectrum is defined as

$$\langle n_I^*(f) n_I(f') \rangle = \frac{1}{2} \delta(f - f') S_I(f). \quad (3.12)$$

The functional forms of the spectra are given by [29, 30]

$$S_A(f) = 8 \sin^2(f/2f_L) \times \left[(2 + \cos(f/f_L)) S_y^{\text{optical-path}} + 2(3 + 2 \cos(f/f_L) + \cos(2f/f_L)) S_y^{\text{proof-mass}} \right], \quad (3.13)$$

$$S_E(f) = S_A(f), \quad (3.14)$$

$$S_T(f) = 2(1 + 2 \cos(f/f_L))^2 \left[S_y^{\text{optical-path}} + 4 \sin^2(f/2f_L) S_y^{\text{proof-mass}} \right], \quad (3.15)$$

^{#4} For the calculation of the overlap reduction function, see [27, 28].

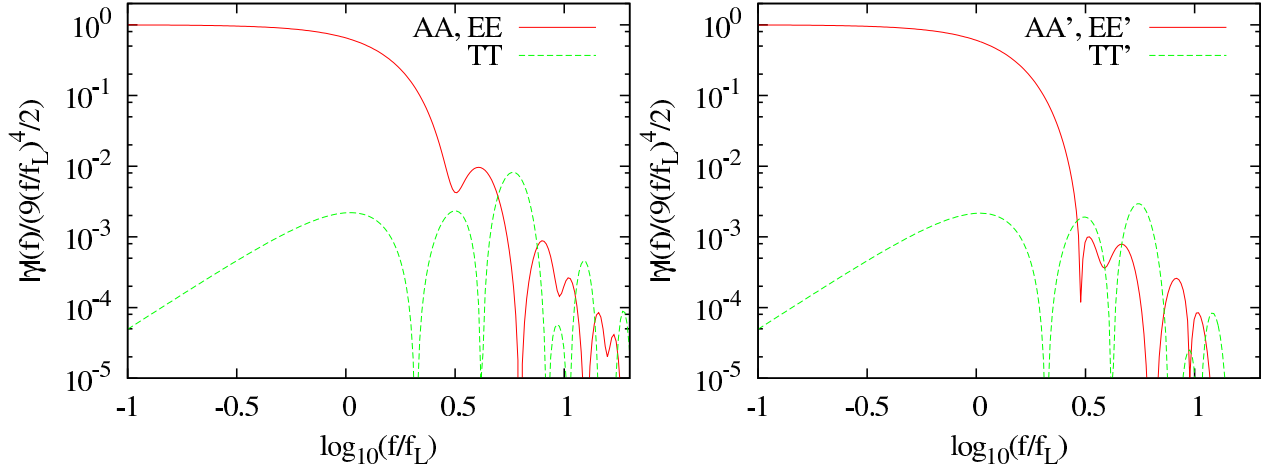


Figure 2: Overlap reduction function $\gamma_{II'}$ for $I = A, E, T$.

Experiments	$L[\text{m}]$	$S_y^{\text{optical-path}}[(f/\text{Hz})^2 \text{ Hz}^{-1}]$	$S_y^{\text{proof-mass}}[(f/\text{Hz})^{-2} \text{ Hz}^{-1}]$
BBO-std	5×10^7	3.6×10^{-49}	2.5×10^{-52}
BBO-grand	2×10^7	1.2×10^{-50}	2.5×10^{-54}
ult-DECIGO	5×10^7	4.7×10^{-51}	4.7×10^{-55}

Table 2: Parameters for the noise power spectra.

where $f_L = c/2\pi L$ with L being the arm length, and $S_y^{\text{optical-path}}$ and $S_y^{\text{proof-mass}}$ parameterize the effects of the optical-path noise and proof-mass noise, respectively. Here, we adopt the noise spectrum for the BBO-standard (abbreviated as BBO-std) and BBO-grand given in [14]. In order to see the result for the ideal situation, we also consider the case where the sensitivity is only limited by the standard quantum limit. In such a case, we adopt the arm length of 5×10^7 m and the mass of 100 kg, and determine $S_y^{\text{optical-path}}$ dominates $S_y^{\text{proof-mass}}$ at the frequency range of $f \gtrsim 0.1$ Hz, assuming that only shot noise contributes to the former; our reference values are $S_y^{\text{optical-path}} = 4.7 \times 10^{-51}(f/\text{Hz})^2 \text{ Hz}^{-1}$ and $S_y^{\text{proof-mass}} = 4.7 \times 10^{-55}(f/\text{Hz})^{-2} \text{ Hz}^{-1}$. (We call this case as ultimate-DECIGO, abbreviated as ult-DECIGO.) The values of $S_y^{\text{optical-path}}$ and $S_y^{\text{proof-mass}}$ used in our analysis are summarized in Table 2.

In our analysis, we use the information about the cross correlation for $(I, I') = (A, A')$, (E, E') , and (T, T') . To see the sensitivities of each experimental setup, we first calculate the spectrum of the IGWs for a given set of fiducial parameters $\{\hat{p}\}$. (In this paper, the “hat” is used for fiducial values.) Using the fact that the noises are uncorrelated for these sets of cross correlations, we calculate $\delta\chi^2$ by postulating the values of the fundamental parameters

$\{p\}$ [31]:

$$\delta\chi^2(\{p\}; \{\hat{p}\}) = -2 \ln \mathcal{L}(\{p\}; \{\hat{p}\}) = \frac{2}{25} T_{\text{obs}} \sum_{(I, I')} \int_{f_{\min}}^{\infty} df \frac{\gamma_{II'}^2(f)}{\sigma_{II'}^2(f)} [S_h(f; \{p\}) - S_h(f; \{\hat{p}\})]^2. \quad (3.16)$$

Here, $S_h(f; \{\hat{p}\})$ and $S_h(f; \{p\})$ are calculated with the fiducial parameters $\{\hat{p}\}$ and the postulated parameters $\{p\}$, respectively, T_{obs} is the observation time, and

$$\sigma_{II'}^2(f) = \left[\frac{1}{2} S_I(f) + \frac{1}{5} \gamma_{II}(f) S_h(f) \right] \left[\frac{1}{2} S_{I'}(f) + \frac{1}{5} \gamma_{I'I'}(f) S_h(f) \right] + \frac{1}{25} \gamma_{II'}^2(f) S_h^2(f). \quad (3.17)$$

We note here that the stochastic cosmic background GWs for $f \lesssim O(0.1 \text{ Hz})$ are expected to be dominated by GWs from white-dwarf binaries, and hence the low-frequency data may not be used for the study of the IGWs. We introduce the minimum frequency f_{\min} to take this fact into account. We will discuss how the result changes as we vary f_{\min} . We can also calculate the signal-to-noise ratio S/N for detection as

$$(S/N)^2 = \frac{2}{25} T_{\text{obs}} \sum_{(I, I')} \int_{f_{\min}}^{\infty} df \frac{\gamma_{II'}^2(f)}{\sigma_{II'}^{(\text{null})2}(f)} [S_h(f; \{\hat{p}\})]^2, \quad (3.18)$$

where $\sigma_{II'}^{(\text{null})}$ is calculated with the assumption of the null signal,

$$\sigma_{II'}^{(\text{null})2}(f) = \frac{1}{4} S_I(f) S_{I'}(f). \quad (3.19)$$

Also, we define the effective strain sensitivity [28]

$$h_{\text{eff}}^{-2}(f) = \left(\frac{2}{25} T_{\text{obs}} f \sum_{(I, I')} \frac{\gamma_{II'}^2(f)}{\sigma_{II'}^{(\text{null})2}(f)} \right)^{1/2}, \quad (3.20)$$

and the effective sensitivity to the GW amplitude $\Delta\Omega_{\text{IGW}}$

$$\Delta\Omega_{\text{IGW}}(f) = \frac{4\pi^2}{3H_0^2} f^3 h_{\text{eff}}^2(f), \quad (3.21)$$

with which

$$(S/N)^2 = \int_{f_{\min}}^{\infty} d \ln f \frac{\Omega_{\text{IGW}}^2(f; \hat{p})}{\Delta\Omega_{\text{IGW}}^2(f)}. \quad (3.22)$$

In Fig. 1, we also plot $\Delta\Omega_{\text{IGW}}$ with $T_{\text{obs}} = 1 \text{ yr}$ for each experiment.

For some fundamental parameters, the likelihood function can be approximated by Gaussian. We collectively denote such parameters by $\{p_a\}$, while denote the other parameters by

$\{p_A\}$. (Here and hereafter, in the subscripts, small letters are used for Gaussian parameters, while capital letters are for non-Gaussian ones.) Then Eq. (3.16) can be expanded as

$$\delta\chi^2(\{p_a, p_A\}; \{\hat{p}\}) = \delta\chi^2(\{p_a^{(\text{ref})}, p_A\}; \{\hat{p}\}) + \sum_{ab} (p_a - p_a^{(\text{ref})})(p_b - p_b^{(\text{ref})}) \mathcal{F}_{ab}(\{p_a^{(\text{ref})}, p_A\}), \quad (3.23)$$

where $\mathcal{F}_{ab}(\{p_a^{(\text{ref})}, p_A\})$ is the Fisher matrix

$$\mathcal{F}_{ab}(\{p_a^{(\text{ref})}, p_A\}) = \frac{2}{25} T_{\text{obs}} \sum_{(I, I')} \int_{f_{\text{min}}}^{\infty} df \frac{\gamma_{II'}^2(f) \partial_{p_a} S_h(f; \{p_a^{(\text{ref})}, p_A\}) \partial_{p_b} S_h(f; \{p_a^{(\text{ref})}, p_A\})}{\sigma_{II'}^2(f)}, \quad (3.24)$$

with ∂_{p_a} being the derivative with respect to the fundamental parameter p_a , and $\{p_a^{(\text{ref})}\}$ is the value of $\{p_a\}$ which gives the minimum of $\delta\chi^2$ for given $\{p_A\}$. In the following analysis we take $\ln \bar{\Omega}_{\text{IGW}}$, n_{T} , α_{T} and T_{R} as fundamental parameters which describe IGWs. As we will see, the likelihood function for the reheating temperature T_{R} cannot be approximated by Gaussian in some cases, thus we take $\{p_a\} = \{\ln \bar{\Omega}_{\text{IGW}}, n_{\text{T}}, \alpha_{\text{T}}\}$ and $\{p_A\} = \{T_{\text{R}}\}$.

To study the expected constraints on the fundamental parameters, we evaluate the likelihood function by using Eq. (3.23). In presenting constraints on above mentioned parameters in two-dimensional plane or one-dimensional axis, we marginalize over irrelevant parameters, which we denote by p_{\perp} collectively, by integrating p_{\perp} as

$$\tilde{\mathcal{L}}(\{p\}; \{\hat{p}\}) = \int dp_{\perp} \mathcal{L}(\{p\}; \{\hat{p}\}). \quad (3.25)$$

(It should be understood that, in the first argument $\{p\}$ of $\tilde{\mathcal{L}}(\{p\}; \{\hat{p}\})$, p_{\perp} is not included.) Then, the $\delta\chi^2$ can be obtained as

$$\delta\chi^2(\{p\}; \{\hat{p}\}) \equiv -2 \ln \frac{\tilde{\mathcal{L}}(\{p\}; \{\hat{p}\})}{\tilde{\mathcal{L}}(\{\hat{p}\}; \{\hat{p}\})}. \quad (3.26)$$

4 Determination of the IGW Spectrum

Now we consider how well we can probe the properties of IGWs using future space-based GW detectors. Throughout this paper, we consider the simplest scenario in which there is no extra entropy production after the decay of inflaton.^{#5}

^{#5}If there exists extra entropy production after the reheating, the IGW spectrum may show significant change compared to the standard case. For example, if there occurred a phase transition in the early universe, the IGW spectrum may show characteristic feature at the frequency corresponding to the time of the cosmic phase transition [32, 33]. The case with late-time entropy production has also been studied in [19, 21]. In any case, we do not consider such a possibility in this paper.

In the following subsections, we show the results of our analysis for the cases with and without including the reheating temperature into the list of fit parameters. In our numerical calculation, we choose the following as fundamental parameters which determine the IGW spectrum:

$$\ln \bar{\Omega}_{\text{IGW}}(f_*), \quad n_{\text{T}}(f_*), \quad \alpha_{\text{T}}(f_*), \quad T_{\text{R}}.$$

(Hereafter we sometimes omit the argument f_* for notational simplicity.) In the following, f_* is optimized in each analysis. (Note that the expected uncertainties in the determination of the fundamental parameters do not change even if we vary the fiducial values within the range shown in Table 1.) In calculating likelihood \mathcal{L} , we assume it to be Gaussian in $\bar{\Omega}_{\text{IGW}}$, n_{T} and α_{T} directions, while we do not in T_{R} direction and use Eq. (3.23).

We use the predictions of the chaotic inflation model with $T_{\text{R}} = 10^{10}$ GeV as the fiducial values, irrespective of the fiducial value of the reheating temperature to make the comparison easier. Then, at 1 Hz,

$$\hat{\bar{\Omega}}_{\text{IGW}}(1 \text{ Hz}) = 1.51 \times 10^{-16}, \quad \hat{n}_{\text{T}}(1 \text{ Hz}) = -0.064, \quad \hat{\alpha}_{\text{T}}(1 \text{ Hz}) = -0.0041. \quad (4.1)$$

The amplitude, the tensor spectral index, and its running at $f = f_*$ are evaluated based on (4.1).

4.1 Case with high enough T_{R}

First, we study the accuracy of the measurements of the parameters $\bar{\Omega}_{\text{IGW}}$, n_{T} , and α_{T} , assuming the shape of the IGW spectrum given in Eq. (2.8) and $\mathcal{T}(f) \rightarrow 1$. This is relevant if the reheating temperature is so high that f_{R} is much larger than the frequency relevant for the GW detectors. We note here that the large tensor-to-scalar ratio recently reported by BICEP2, together with the scalar amplitude and the e -folding, is consistent with the chaotic inflation model with the mass scale m_{ϕ} of order 10^{13} GeV. Such a value of m_{ϕ} results in the reheating temperature as high as $\sim 10^{10}$ GeV if the inflaton couples to the standard-model sector via Planck-suppressed operator, which gives f_{R} much higher than 1 Hz. Thus, for such a case, the analysis given in this subsection is relevant.

We calculate the likelihood as a function of $\{p\} = \{\log_{10} \bar{\Omega}_{\text{IGW}}, n_{\text{T}}, \alpha_{\text{T}}\}$. In the left panels of Figs. 3 – 4, we show the contours of constant $\delta\chi^2 = 5.99$ (corresponding to 95 % C.L.) on the $\bar{\Omega}_{\text{IGW}}$ vs. n_{T} and n_{T} vs. α_{T} planes.^{#6} In each figure, the noise level of BBO-std, BBO-grand, or ult-DECIGO is adopted, and the lowest frequency f_{min} is taken to be 0.1 Hz.

First, we consider the determination of $\bar{\Omega}_{\text{IGW}}$ and n_{T} . As we will see below, the uncertainty of α_{T} becomes comparable to or larger than that of n_{T} . On the contrary, in slow-roll inflation model, $|\alpha_{\text{T}}|$ is expected to be much smaller than $|n_{\text{T}}|$. This implies that, assuming slow-roll inflation, the running is (almost) irrelevant for the determination of $\bar{\Omega}_{\text{IGW}}$ and n_{T} . Thus, we first discuss the result based on the analysis with $\{p\} = \{\log_{10} \bar{\Omega}_{\text{IGW}}, n_{\text{T}}\}$ and α_{T}

^{#6}Here and hereafter, axes of some of the panels are extended to very large values, like $n_{\text{T}} \sim \mathcal{O}(1)$ and $\alpha_{\text{T}} \sim 10$. These are taken just for demonstrative purposes, although they are unnaturally large.

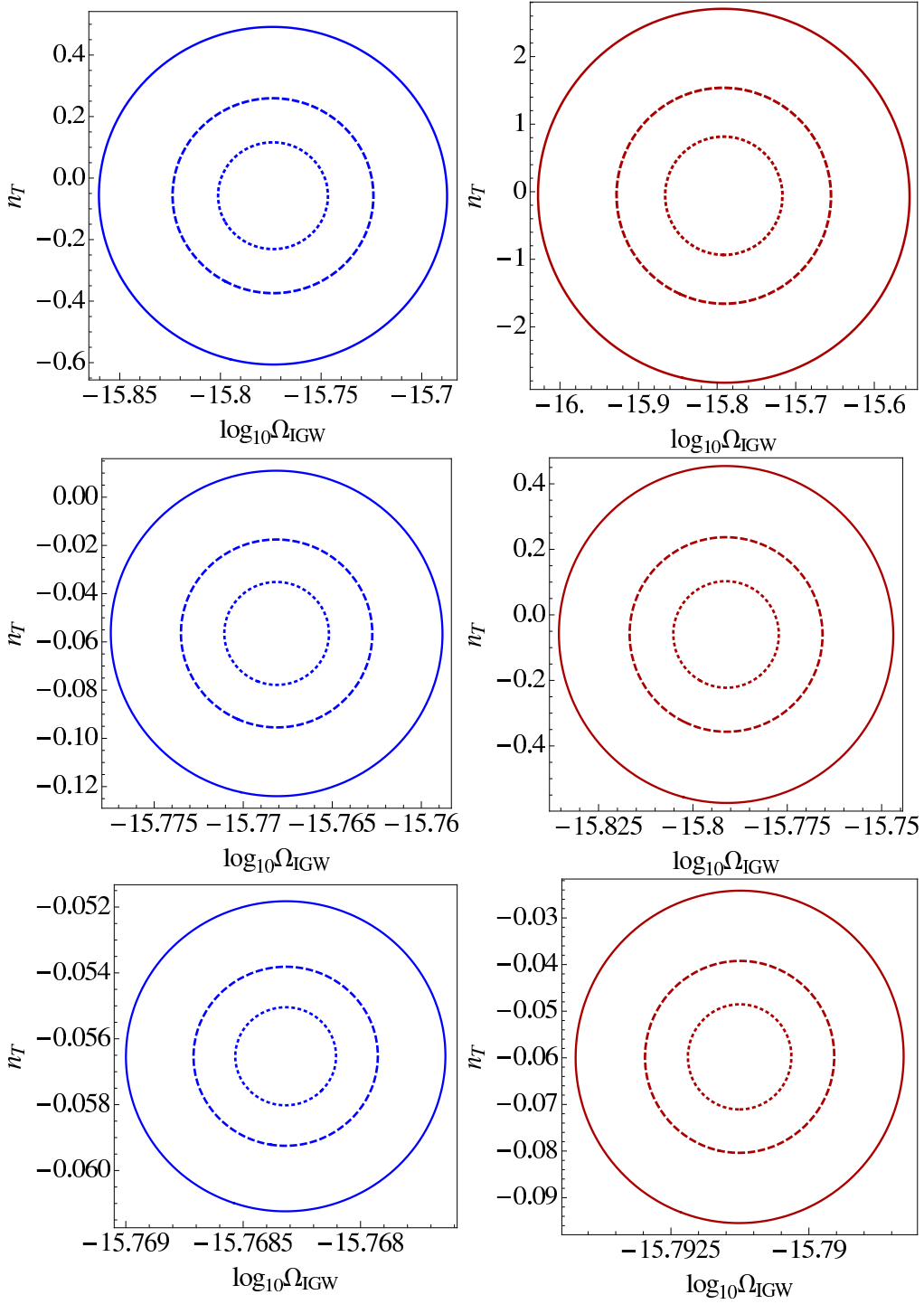


Figure 3: 95% C.L. expected constraints on the $\log_{10} \bar{\Omega}_{\text{IGW}}$ vs. n_{T} plane for BBO-std (top), BBO-grand (middle) and ult-DECIGO (bottom). In these figures, $\log_{10} \bar{\Omega}_{\text{IGW}}$ and n_{T} are varied while α_{T} is fixed to the fiducial value. The minimum frequency f_{min} is taken to be 0.1 Hz (left panels with blue contours) and 0.3 Hz (right panels with red contours). The solid (dashed, dotted) line corresponds to $T_{\text{obs}} = 1$ yr, (3 yr, 10 yr).

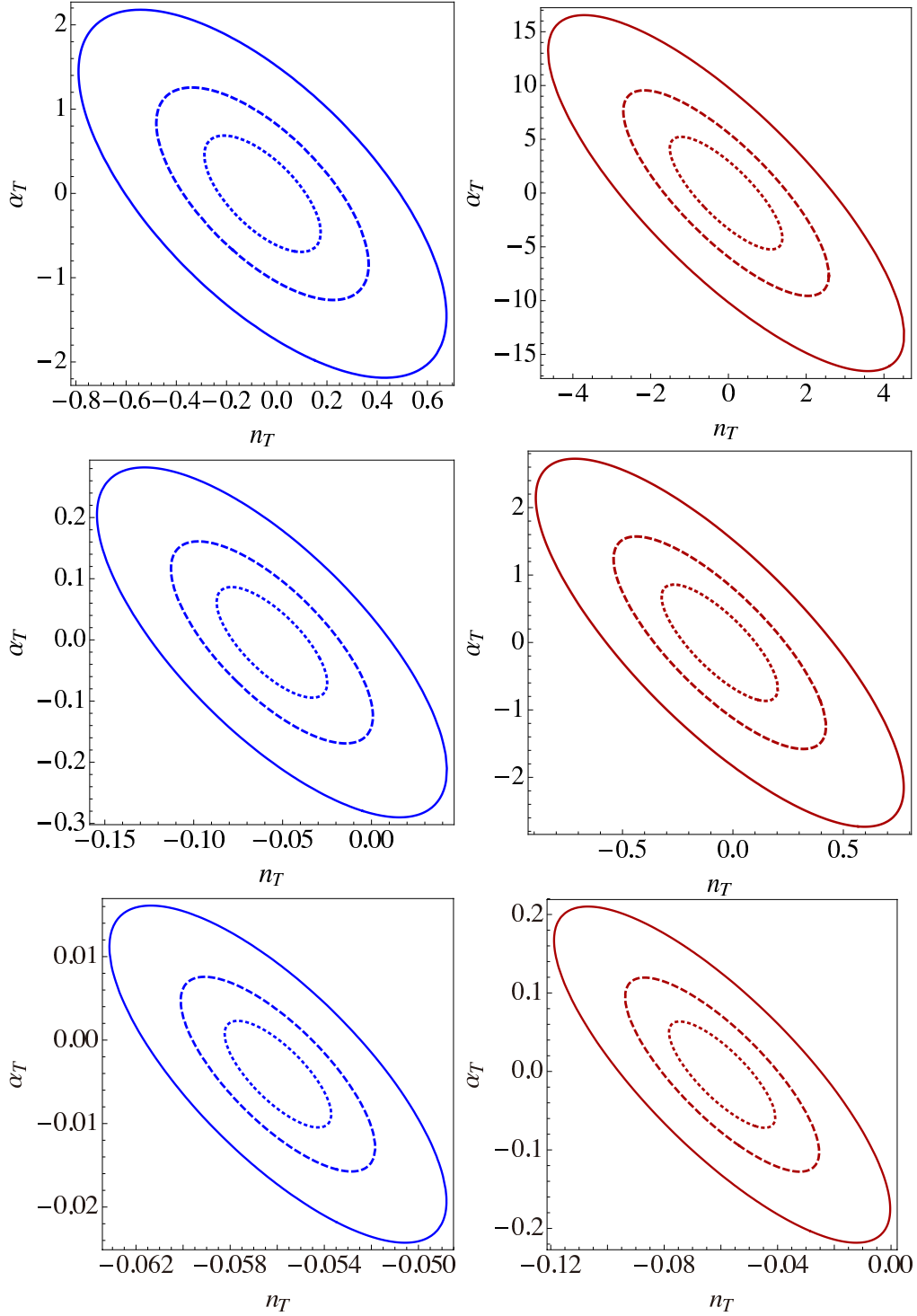


Figure 4: 95% C.L. expected constraints on the n_T vs. α_T plane for BBO-std (top), BBO-grand (middle) and ult-DECIGO (bottom). In these figures, $\log_{10} \bar{\Omega}_{\text{IGW}}$ is marginalized. The minimum frequency f_{min} is taken to be 0.1 Hz (left panels with blue contours) and 0.3 Hz (right panels with red contours). The solid (dashed, dotted) line corresponds to $T_{\text{obs}} = 1$ yr, (3 yr, 10 yr).

being fixed to the fiducial value. Here we note that $\{p\}$ depends on the pivot scale f_* , i.e. $\{p\} = \{p(f_*)\}$. We can make the correlation between $\ln \Omega_{\text{IGW}}$ and n_{T} vanish by properly choosing f_* ; for such a choice of f_* , the error of $\bar{\Omega}_{\text{IGW}}$ is minimized if we neglect α_{T} .^{#7} Thus in the following we choose such f_* for each experiment and each f_{min} , and the value is summarized in Table 3.

On $\bar{\Omega}_{\text{IGW}}$, a relatively good determination of $\bar{\Omega}_{\text{IGW}}$ is possible even with the noise level of BBO-std [14]. (See the top panels of Fig. 3.) With a better noise level, like BBO-grand and ult-DECIGO, more precise measurement of $\bar{\Omega}_{\text{IGW}}$ is expected. (See the middle and bottom of the same figure.) From the Fisher matrix, we estimate the error in the determination of $\bar{\Omega}_{\text{IGW}}$; taking $T_{\text{obs}} = 10$ yr, the 1σ error is found to be 2.6 %, 0.28 %, and 0.020 % for BBO-std, BBO-grand, and ult-DECIGO, respectively, after marginalizing n_{T} . The errors with other choices of fundamental parameters are summarized in Table 4.

The error of n_{T} can be also understood from Fig. 3. We also calculate the error of n_{T} for each detector parameters; the results are summarized in Table 4. We can see that, even with the noise level of BBO-std, n_{T} may be known to be $O(0.01)$. If such a result becomes available, it will tell us that the slow-roll condition is likely to be satisfied when the mode with $f \sim 0.1$ Hz exits the horizon during inflation. It is notable that, with the noise level of BBO-grand, the uncertainty of n_{T} becomes comparable to the fiducial value (if we adopt the prediction of the chaotic inflation). This fact implies that, with such a sensitivity, we may be able to detect the tensor spectral index which provides a very important information about the slow-roll parameter. Then, with ult-DECIGO, the error of n_{T} can be $\lesssim 10^{-3}$.

In order to estimate the expected sensitivity of the running (as well as others), we also calculate the likelihood taking $\{p\} = \{\log_{10} \bar{\Omega}_{\text{IGW}}, n_{\text{T}}, \alpha_{\text{T}}\}$. The result is shown in Fig. 4. In making these figures we chose f_* for which the correlation between $\bar{\Omega}_{\text{IGW}}$ and n_{T} vanishes after marginalizing α_{T} . Here we show only the n_{T} vs. α_{T} plane after marginalizing $\log_{10} \bar{\Omega}_{\text{IGW}}$, since the $\bar{\Omega}_{\text{IGW}}$ vs. n_{T} plane with α_{T} being marginalized is roughly the same as Fig. 3 (about $O(10\%)$ difference in the error of each parameter). We can see that, with the noise level of BBO-std, the error in α_{T} is orders of magnitude larger than the expectation from slow-roll inflation. With the noise level of BBO-grand, on the contrary, we may obtain

^{#7}For notational simplicity, let us denote $x_0 = \ln \bar{\Omega}_{\text{IGW}} - \ln \hat{\Omega}_{\text{IGW}}$ and $x_1 = n_{\text{T}} - \hat{n}_{\text{T}}$. Then, neglecting α_{T} , the amplitude and the tensor spectral index for two different pivot scales, f_* and f'_* , are related as

$$x'_0 = x_0 + x_1 \ln(f'_*/f_*), \quad x'_1 = x_1,$$

where the quantities without (with) the prime are evaluated at f_* (f'_*). (See Eqs. (2.6) and (2.7).) The error of x'_0 is given by

$$\langle x'^2_0 \rangle = \langle x^2_0 \rangle + 2 \ln(f'_*/f_*) \langle x_0 x_1 \rangle + \ln^2(f'_*/f_*) \langle x^2_1 \rangle,$$

where $\langle \dots \rangle$ denotes the expectation value calculated with Gaussian probability density. Then, $\langle x'^2_0 \rangle$ is minimized when

$$\ln(f'_*/f_*) = -\langle x_0 x_1 \rangle / \langle x^2_1 \rangle.$$

With such a choice of f'_* , $\langle x'_0 x'_1 \rangle = 0$, and hence x'_0 and x'_1 become uncorrelated.

	BBO-std 0.1/0.3Hz	BBO-grand 0.1/0.3Hz	ult.-DECIGO 0.1/0.3Hz
$\Omega_{\text{IGW}}, n_{\text{T}}$	0.20/0.37	0.16/0.37	0.17/0.37
$\Omega_{\text{IGW}}, n_{\text{T}}, \alpha_{\text{T}}$	0.17/0.35	0.15/0.35	0.14/0.35

Table 3: f_* [Hz] for each experiment and for each cutoff frequency.

	BBO-std 0.1/0.3Hz	BBO-grand 0.1/0.3Hz	ult.-DECIGO 0.1/0.3Hz
S/N	39/14	$3.6 \times 10^2/76$	$4.9 \times 10^3/1.1 \times 10^3$
$\log_{10} \Omega_{\text{IGW}}$	$1.1 \times 10^{-2}/3.1 \times 10^{-2}$	$1.2 \times 10^{-3}/5.7 \times 10^{-3}$	$8.8 \times 10^{-5}/3.8 \times 10^{-4}$
$\log_{10} \bar{\Omega}_{\text{IGW}} \text{ (w}/n_{\text{T}})$	$1.4 \times 10^{-2}/3.3 \times 10^{-2}$	$1.4 \times 10^{-3}/6.1 \times 10^{-3}$	$1.0 \times 10^{-4}/4.2 \times 10^{-4}$
$\log_{10} \bar{\Omega}_{\text{IGW}} \text{ (w}/n_{\text{T}}, \alpha_{\text{T}})$	$1.3 \times 10^{-2}/3.3 \times 10^{-2}$	$1.4 \times 10^{-3}/6.1 \times 10^{-3}$	$1.0 \times 10^{-4}/4.1 \times 10^{-4}$
$n_{\text{T}} \text{ (w}/\log_{10} \bar{\Omega}_{\text{IGW}})$	$7.1 \times 10^{-2}/0.36$	$8.7 \times 10^{-3}/6.6 \times 10^{-2}$	$6.1 \times 10^{-4}/4.6 \times 10^{-3}$
$n_{\text{T}} \text{ (w}/\log_{10} \bar{\Omega}_{\text{IGW}}, \alpha_{\text{T}})$	$9.5 \times 10^{-2}/0.59$	$1.3 \times 10^{-2}/0.11$	$9.3 \times 10^{-4}/7.7 \times 10^{-3}$
$\alpha_{\text{T}} \text{ (w}/\log_{10} \bar{\Omega}_{\text{IGW}}, n_{\text{T}})$	0.28/2.1	$3.7 \times 10^{-2}/0.35$	$2.6 \times 10^{-3}/2.8 \times 10^{-2}$

Table 4: 1σ error for each parameter with the lowest frequency $f_{\text{min}} = 0.1$ and 0.3 Hz. Here, we take $T_{\text{obs}} = 10$ yr. (Notice that the errors scale as $T_{\text{obs}}^{-1/2}$.) In the parenthesis, the parameters marginalized are listed.

a bound on $|\alpha_{\text{T}}|$ of $\lesssim 0.1$ if the operation time of ~ 10 yr is adopted. If the noise level of ult-DECIGO is available, we have a stronger bound of $\lesssim 0.01$.

So far, we have shown the results for $f_{\text{min}} = 0.1$ Hz. However, we should note here that the accuracy of the parameter determination strongly depends on the lowest frequency f_{min} . To see what happens if we take larger value of f_{min} , we also calculate the likelihood with $f_{\text{min}} = 0.3$ Hz. The results for BBO-std, BBO-grand and ult-DECIGO are shown in the right panels of Figs. 3 – 4. As we can see, larger value of f_{min} results in a worse measurement of the fundamental parameters. This is because the signal-to-noise ratio becomes largest for $f \sim O(0.1 \text{ Hz})$. As we have mentioned, the value of f_{min} reflects the expectation that the density of the GWs from white-dwarf binaries is much larger than that of IGWs. Better understanding of the former would help to improve the study of the IGWs.

To distinguish α_{T} from 0, we need a more sensitive detector than ult-DECIGO. Since the standard quantum limit depends on L and m , we consider the case with $L = 5 \times 10^8$ km and $m = 500$ kg, for example. Then, assuming that the noise level is limited only by the standard quantum limit and that the shot noise dominates the frequency range of $f > 0.1$ Hz, we take

$$S_y^{\text{optical-path}} = 9.3 \times 10^{-52} [(f/\text{Hz})^2 \text{ Hz}^{-1}], \quad (4.2)$$

$$S_y^{\text{proof-mass}} = 9.3 \times 10^{-56} [(f/\text{Hz})^{-2} \text{ Hz}^{-1}]. \quad (4.3)$$

The expected constraint on the n_{T} vs. α_{T} plane (with $f_{\text{min}} = 0.1$ Hz and $f_* = 0.17$ Hz) is shown in Fig. 5. With such a noise level, non-vanishing value of α_{T} may be seen; then, combining the information about α_{T} and n_{T} , the slow-roll parameters ϵ and η can be reconstructed, which would become a very important discriminator of various inflation models.

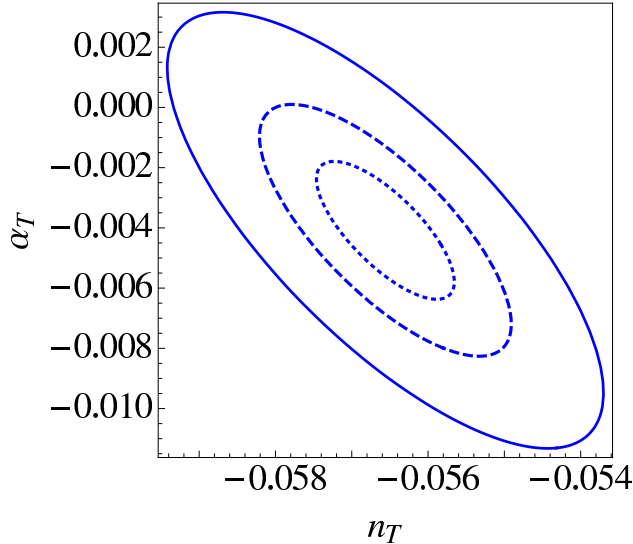


Figure 5: 95 % C.L. expected constraints on the n_T vs. α_T plane for the detector parameters given in Eqs. (4.2) and (4.3) with $f_{\min} = 0.1$ Hz. The solid (dashed, dotted) line corresponds to $T_{\text{obs}} = 1$ yr, (3 yr, 10 yr). The pivot scale is taken to be $f_* = 0.17$ Hz.

4.2 Determination of T_R

Next, we include T_R into the fit parameters, paying particular attention to the determination of T_R . As we have mentioned, the IGW spectrum for $f \gtrsim f_R$ is significantly suppressed. If such a behavior can be confirmed by GW detectors, we have a possibility to acquire the information about the reheating temperature [16–21]. It should be, however, also noted that the change of the shape of the IGW spectrum may affect the determinations of other fundamental parameters, in particular, $\bar{\Omega}_{\text{IGW}}$ and n_T . In this subsection, we consider how well we can determine the shape of the IGWs, taking $\bar{\Omega}_{\text{IGW}}$, n_T , and T_R as fundamental parameters. In this analysis, we do not include the parameter α_T , because $|\alpha_T|$ is expected to be small in slow-roll inflation model. Also, we choose the pivot scale f_* to be the same value as adopted in the analysis with $\bar{\Omega}_{\text{IGW}}$ and n_T in the previous subsection (see Table 3).

If the reheating temperature is relatively low, the IGW amplitude in the frequency range relevant for the GW detectors is suppressed, as we have discussed in Section 2. Then, with low reheating temperature, the detection of the IGW signal becomes difficult. To see this, in Fig. 6, we show the signal-to-noise ratio as a function of T_R . As one can see, the detection of the IGW spectrum is possible only if $T_R \gtrsim 10^5 - 10^6$ GeV. Thus, in the following, we concentrate on the case where the reheating temperature is higher than 10^6 GeV.

We calculated the likelihood as a function of $\bar{\Omega}_{\text{IGW}}$, n_T , and T_R for the case where the signal-to-noise ratio is large enough for the detection. Here, $p_i^{(\text{ref})}$ is taken to be the point where \mathcal{L} is minimized for the fixed value of T_R . In Figs. 7 – 12, we show the contours of $\delta\chi^2 = 5.99$ on the T_R vs. $\bar{\Omega}_{\text{IGW}}$ and T_R vs. n_T planes, taking the fiducial value of the

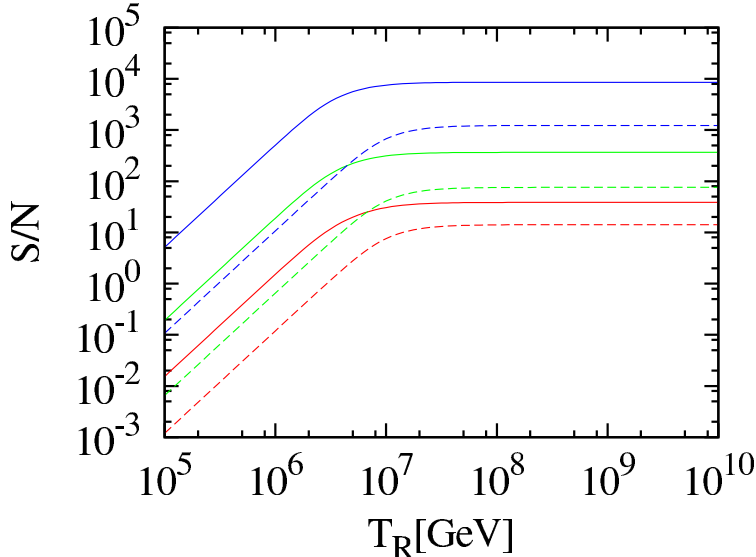


Figure 6: Signal-to-noise ratio as a function of the reheating temperature. The IGW spectrum is calculated with $\bar{\Omega}_{\text{IGW}} = 1.51 \times 10^{-16}$, and $n_{\text{T}} = -6.38 \times 10^{-2}$. Each line corresponds to BBO-std (red), BBO-grand (green) and ult-DECIGO (blue), respectively, and the solid and dashed lines are for $f_{\text{min}} = 0.1$ and for 0.3 Hz, respectively. The observation time is taken to be $T_{\text{obs}} = 10$ yr.

reheating temperature to be 10^7 GeV or 10^9 GeV.^{#8}

We first show the behavior of $\delta\chi^2$ with n_{T} being fixed to be the fiducial value; the result is shown on the T_{R} vs. $\bar{\Omega}_{\text{IGW}}$ plane (top panels). These figures indicate that, if we impose $|n_{\text{T}}| \ll 1$, T_{R} is always bounded from below irrespective of the fiducial value of the reheating temperature (as far as the signal is detected). We also show the contours of $\delta\chi^2 = 5.99$ with n_{T} being marginalized (middle figure); no prior for n_{T} is imposed in the calculation for these figures. We can see that the accuracy of the determination of fundamental parameters becomes drastically worse if we marginalize n_{T} . In particular, for the case of $\hat{T}_{\text{R}} = 10^7$ GeV, the allowed parameter space extends to the region of low reheating temperature (and high value of $\bar{\Omega}_{\text{IGW}}$) for some choices of noise parameters. This behavior can be understood as follows. If the postulated value of T_{R} is lower than the fiducial one, the postulated IGW spectrum decreases more rapidly than the fiducial one with the increase of f . Such a discrepancy can be compensated by adopting a highly blue-tilted IGW spectrum, i.e., large and positive value of n_{T} . (See also the behavior of $\delta\chi^2$ on the T_{R} vs. n_{T} plane.) To see this, we also show the contours of the best-fit value of n_{T} to be zero on the T_{R} vs. $\bar{\Omega}_{\text{IGW}}$ plane (black-dashed lines in middle panels). We can see that relatively high value of the tensor spectral index (i.e., $n_{\text{T}} \sim 1$) is needed in some region to make the fiducial and postulated spectra consistent. This fact implies that, if a prior for n_{T} is imposed, we may obtain a

^{#8}In some figures, like Figs. 8 and 9, the allowed region shows island-like behavior. They are the consequence of the poor data sampling in our numerical calculation due to our limitation of the computational power.

lower bound on the reheating temperature even if n_T is marginalized. In simple slow-roll inflation models, the expansion rate during inflation decreases with time, which results in a negative value of n_T . Concentrating on the parameter region with $n_T < 0$, for example, the cases with and without the marginalization of n_T give similar lower bounds on the reheating temperature. We also note here that, if the reheating temperature is too high, the reheating temperature is bounded only from below. (See figures for $\hat{T}_R = 10^9$ GeV.) This is because, with high enough reheating temperature, f_R becomes much larger than ~ 1 Hz so that the shape of the IGW spectrum for the frequency relevant for the GW detectors becomes almost flat.

The contours of constant $\delta\chi^2$ on the T_R vs. n_T plane, with the marginalization of $\log_{10} \bar{\Omega}_{\text{IGW}}$, are also shown (bottom panels); no prior for $\log_{10} \bar{\Omega}_{\text{IGW}}$ is imposed in the calculation for these figures. Assuming that the expansion rate during inflation decreases with time, precise determination of the tensor-to-scalar ratio at the CMB scale imposes upper bound on $\bar{\Omega}_{\text{IGW}}$. In the figures, we also show the contour on which the best-fit value of $\bar{\Omega}_{\text{IGW}}$ becomes equal to 5×10^{-16} , which is the value given by the tensor-to-scalar ratio at the CMB scale of 0.15 (which is the prediction of the chaotic inflation model).

We can see that the accuracy of the determination of the tensor spectral index is poor in particular when the reheating temperature is relatively low (see the figures with $\hat{T}_R = 10^7$ GeV). This is because of the suppression of the IGW spectrum for $f \gtrsim f_R$; such a behavior may be mimicked by tilting the spectrum. However, if the reheating temperature is high enough, the accuracy of the determination of n_T does not change so much (see the figures with $\hat{T}_R = 10^9$ GeV). ^{#9}

We also compare our results with those of Fisher analysis. For this purpose, we calculate the Fisher matrix in the parameter space of $\{p_i\} = \{\log_{10} \bar{\Omega}_{\text{IGW}}, n_T, \ln T_R\}$. 95 % C.L. bound with the Fisher analysis is also shown in Figs. 7 – 12 as pink-shaded regions. When the fundamental parameters are well constrained, two analyses give more or less similar bounds. When the error in the measurement become sizable, on the contrary, this is not the case. In particular, if the fiducial value of the reheating temperature is so high that T_R can be bounded only from below, constraints from two analyses show significant difference. This is mainly because the Gaussian approximation discussed in Section 3 breaks down when the postulated value of the reheating temperature becomes much smaller or larger than the fiducial value (see Figs. 10 – 12). Thus, for the precise determination of the bounds on the reheating temperature, analysis based on the full likelihood function is suggested.

Finally, we also show the expected accuracy of the determination of T_R . In Fig. 13, we show the expected upper and lower limits of T_R as functions of the fiducial value of T_R for $f_{\text{min}} = 0.1$ Hz (left) and 0.3 Hz (right). In these figures, the observation time is assumed to

^{#9} In Figs. 7 – 12, we do not show the contours which correspond to particular confidence levels. This is because of the following reasons. First, in some values of \hat{T}_R , the likelihood function does not converge to 0 sufficiently for $T_R \rightarrow \infty$. The contours of particular confidence levels in such cases are sensitive to the prior region of $\ln T_R$ which we choose, and thus may not be reasonable ones. Second, these contours also depends on whether T_R or $\ln T_R$ is considered as the fundamental parameter. For the same reason, we define the upper and lower limit of T_R by the value of $\delta\chi^2$ in Fig. 13.

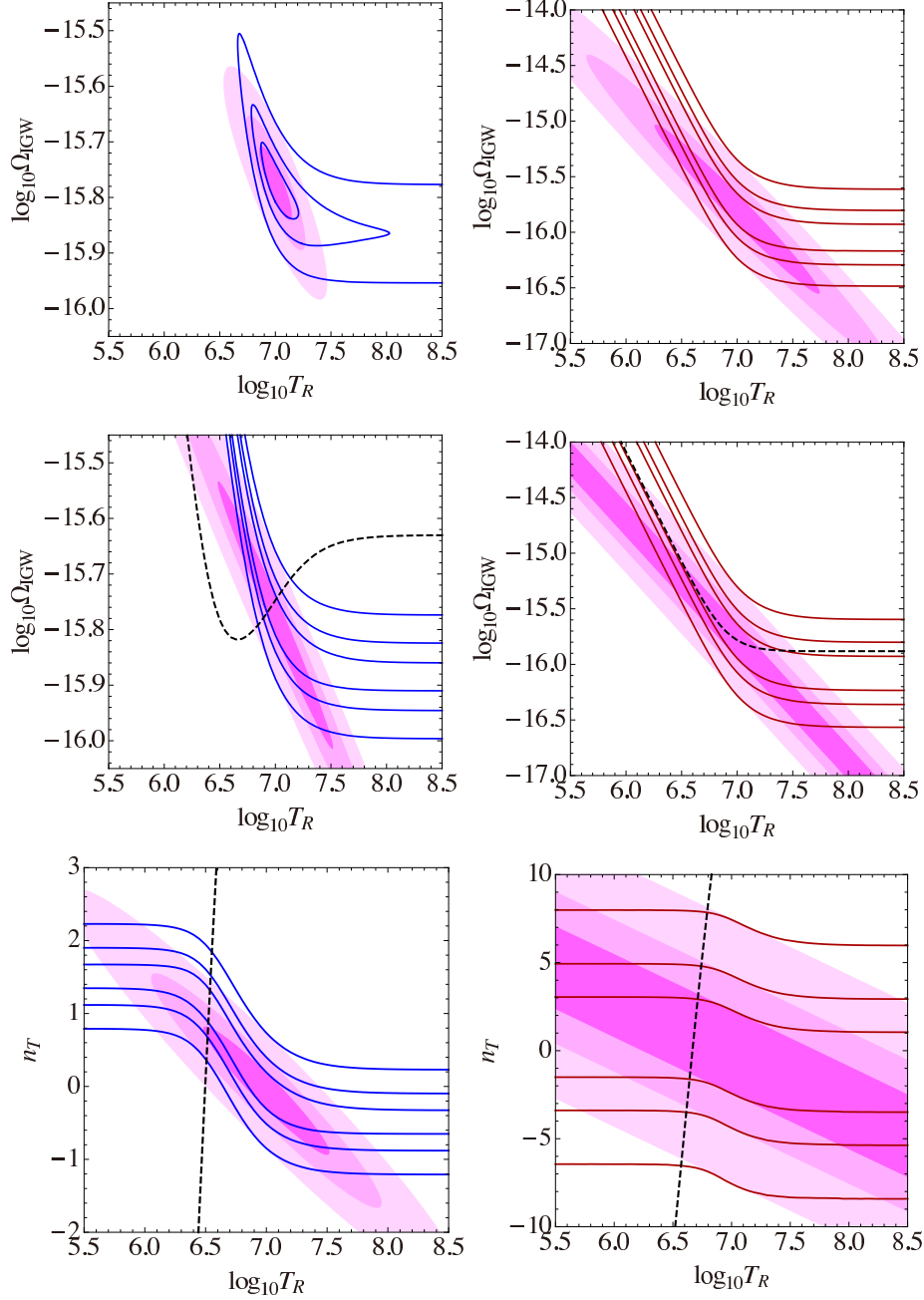


Figure 7: The solid lines are the contours of $\delta\chi^2 = 5.99$ with the fiducial values of $T_R = 10^7$ GeV. The noise function of BBO-std is adopted with $T_{\text{obs}} = 1, 3, \text{ and } 10$ yr (from outside to inside), and $f_{\text{min}} = 0.1$ (left panels with blue lines) and 0.3 Hz (right panels with red lines). Pink regions are the results in the case where T_R is also included in the Fisher analysis. Top: case with n_T being fixed to be the fiducial value. Middle: case with n_T being marginalized. The dashed line corresponds to the contour on which the best-fit value of n_T becomes 0. Bottom: case with $\bar{\Omega}_{\text{IGW}}$ being marginalized. The dashed line corresponds to the contour on which the best-fit value of $\bar{\Omega}_{\text{IGW}}$ becomes 5×10^{-16} .

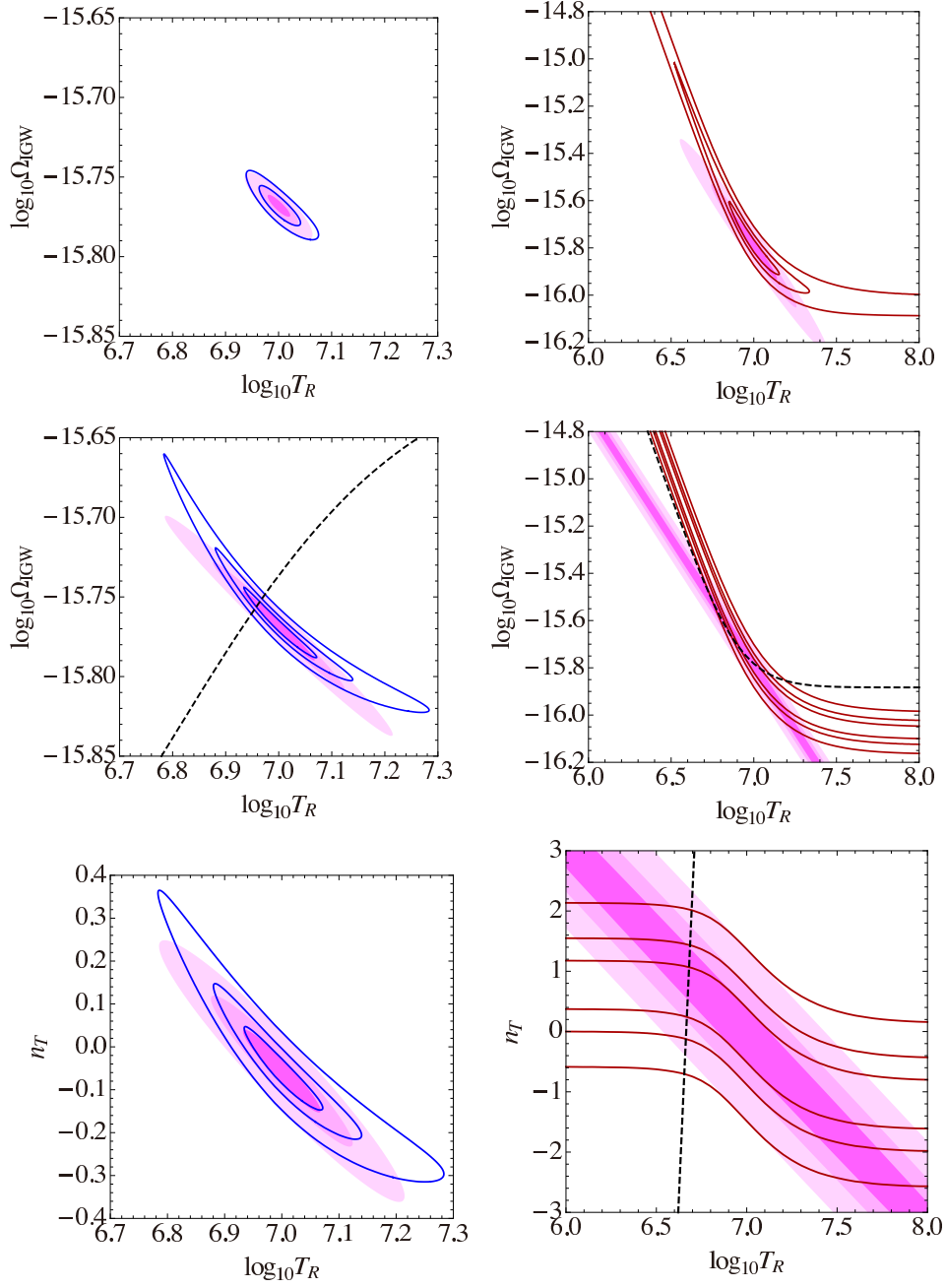


Figure 8: Same as Fig. 7, except that the noise function for BBO-grand is used.

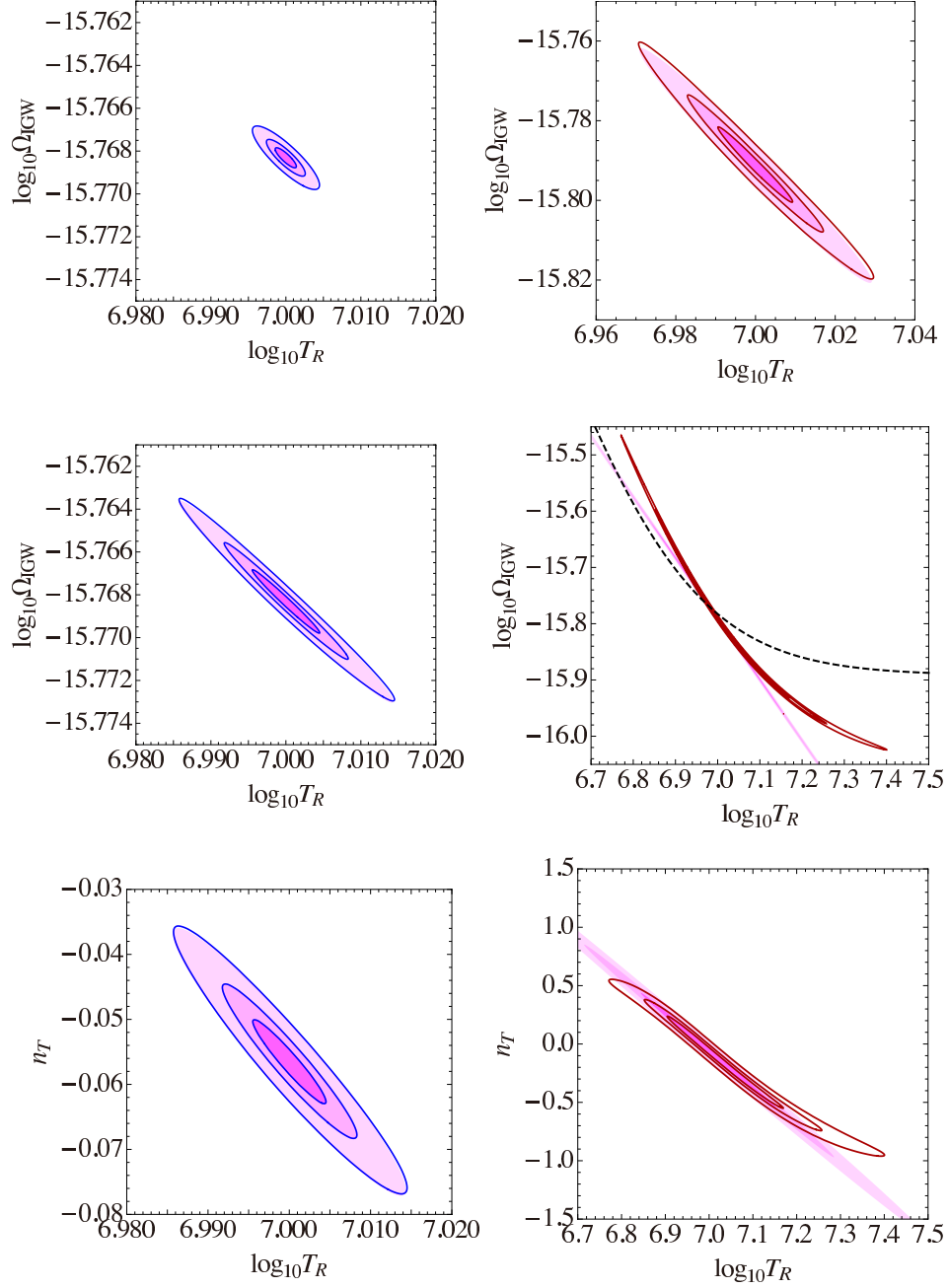


Figure 9: Same as Fig. 7, except that the noise function for ult-DECIGO is used.

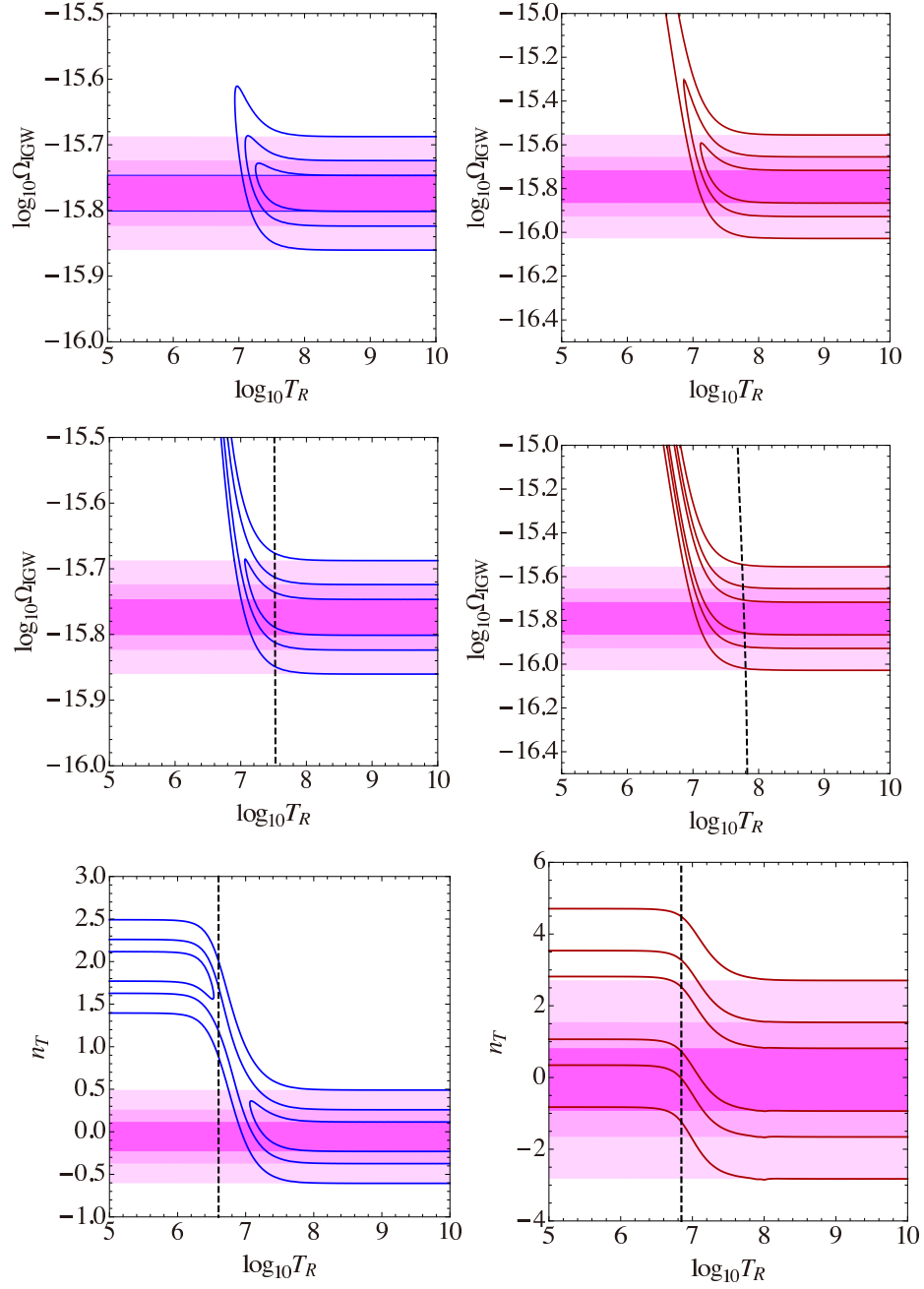


Figure 10: Same as Fig. 7, except for $T_R = 10^9 \text{ GeV}$.

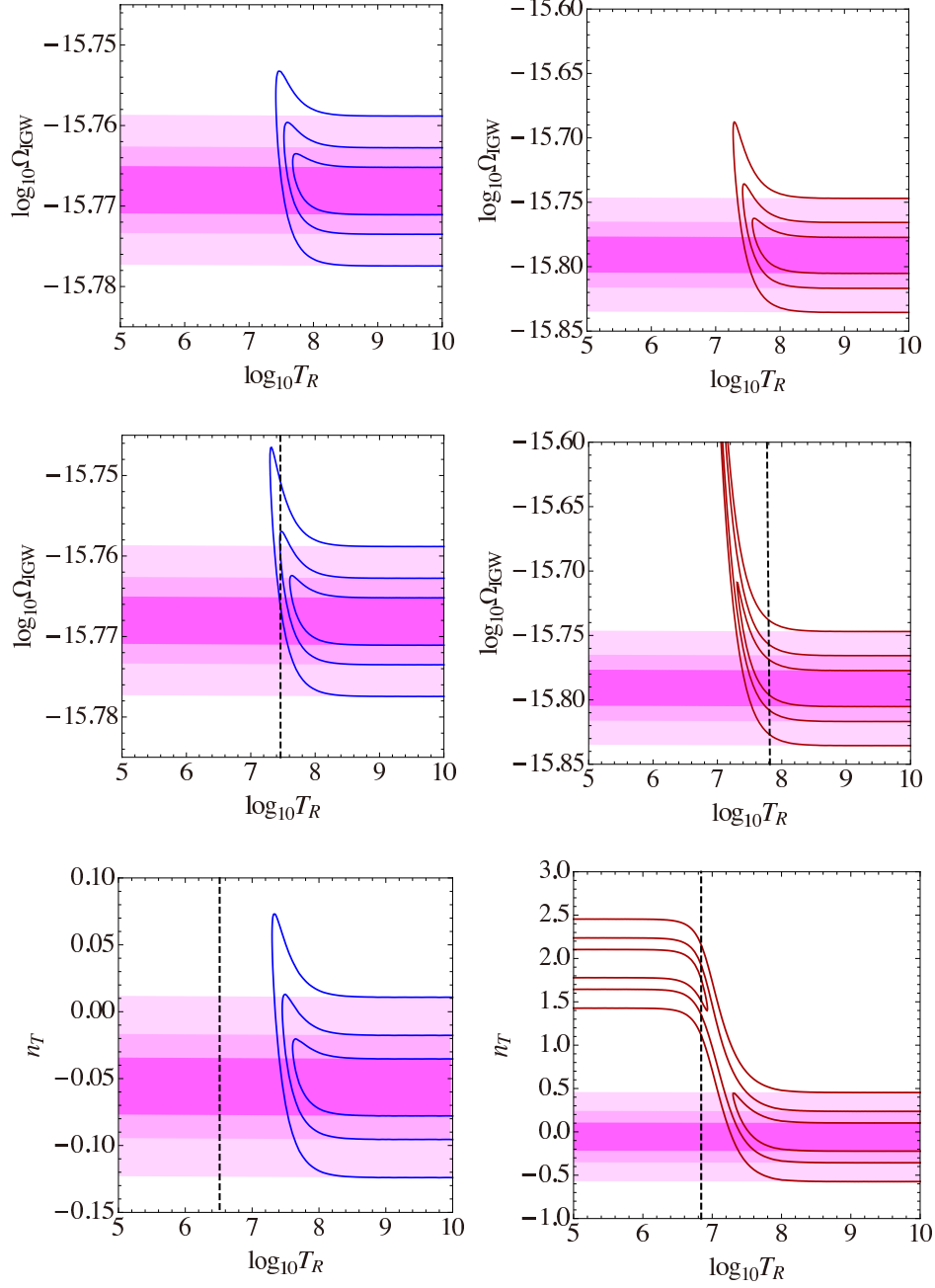


Figure 11: Same as Fig. 7, except for $T_R = 10^9 \text{ GeV}$ and that the noise function for BBO-grand is used.

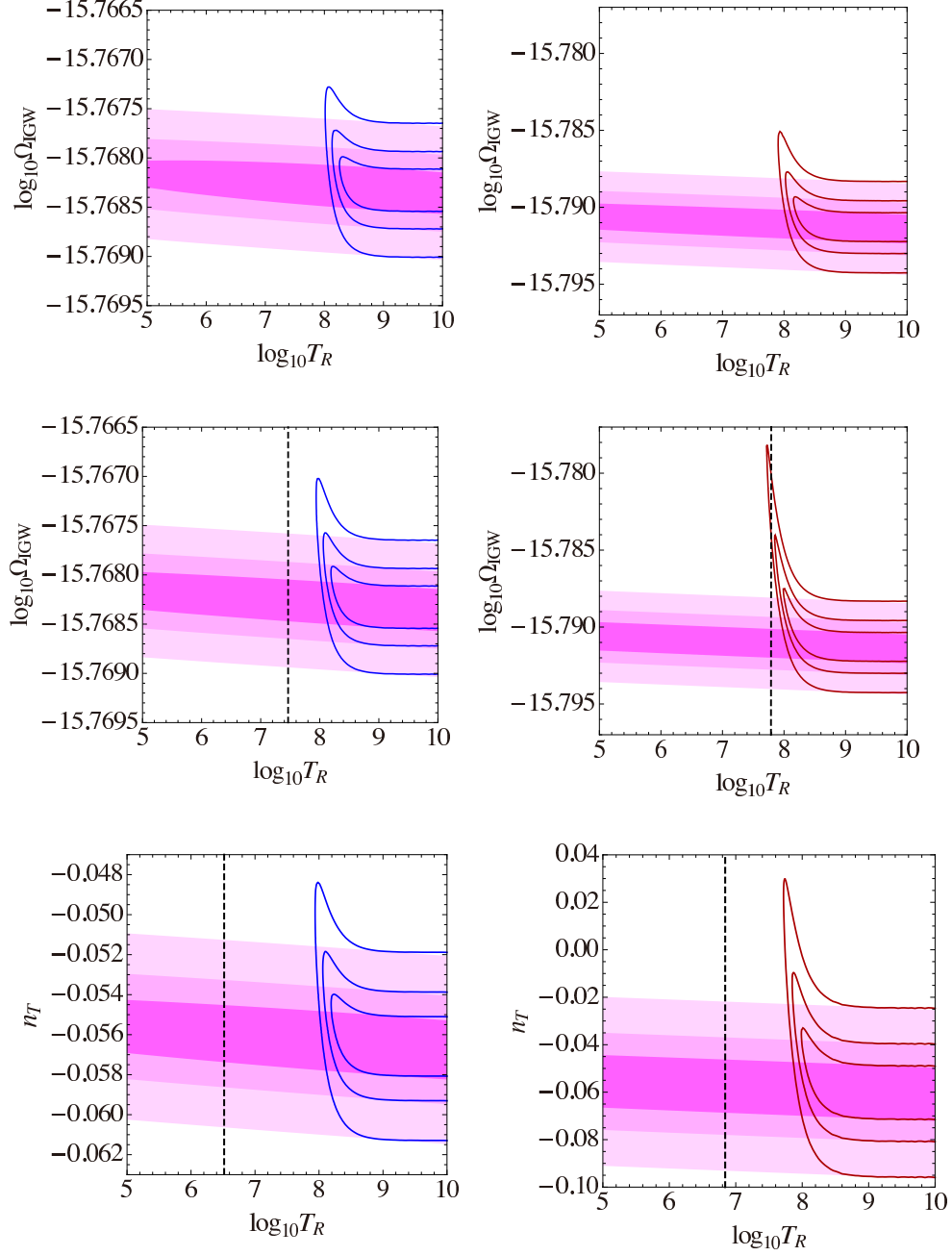


Figure 12: Same as Fig. 7, except for $T_R = 10^9 \text{ GeV}$ and that the noise function for ult-DECIGO is used.

be $T_{\text{obs}} = 10$ yr. Also, the upper and lower limits are defined as the postulated T_R which gives $\delta\chi^2 = 4$ after the marginalization of $\ln\bar{\Omega}_{\text{IGW}}$ and n_T . Here, in order to set the prior for $\ln\Omega_{\text{IGW}}(f)$, we adopt a mild assumption that $\Omega_{\text{IGW}}(f)$ decreases with frequency, which is the case in slow-roll inflation models. Requiring that $\Omega_{\text{IGW}}(f)$ at the scale relevant for the GW detector does not exceed that at the CMB scale, we assume a flat prior for $\ln\Omega_{\text{IGW}}(f)$ in $[-\infty, -15.3]$. (The upper bound corresponds to $\bar{\Omega}_{\text{IGW}} = 5 \times 10^{-16}$.) In addition, n_T is fixed to be the fiducial value in the top panels while we adopt a flat prior in $[-0.1, 0]$ (middle) or $[-\infty, 0]$ (bottom) in other panels.

From the top-left panels of Fig. 13, one can see that T_R is bounded from both below and above with the sensitivity of BBO-std for $10^{6.5} \text{ GeV} \lesssim T_R \lesssim 10^7 \text{ GeV}$, if $f_{\text{min}} = 0.1 \text{ Hz}$ and n_T is fixed to the fiducial value. With better noise levels like BBO-grand and ult-DECIGO, such a region for T_R becomes broader. For higher \hat{T}_R only a lower bound is obtained, and this is consistent with the left panels of Figs. 10 – 12. If $|n_T|$ is required to be much smaller than 1, the qualitative behaviors of the bounds are more or less the same (see the case with the marginalization of n_T for $[-0.1, 0]$). If the marginalization is for $[-\infty, 0]$, on the contrary, the upper bound becomes significantly worse. In particular, the upper bound cannot be obtained with the noise level of BBO-std. We can also see that the bounds are strongly dependent on the minimum frequency f_{min} . One can see that the bounds with $f_{\text{min}} = 0.3 \text{ Hz}$ are much worse than those with $f_{\text{min}} = 0.1 \text{ Hz}$.^{#10}

5 Testing Chaotic Inflation

With the determination of $\bar{\Omega}_{\text{IGW}}$, n_T and α_T (as well as T_R), information about the properties of inflaton may be obtained. Thus, we briefly discuss the implication of the determination of the IGW spectrum for the test of inflation models. If we take the chaotic inflation model we have introduced in Section 2 as the model of inflation, the properties of the inflaton can be parameterized by two parameters, the inflaton mass m_ϕ and the decay rate Γ_ϕ (or equivalently, the reheating temperature). If the reheating temperature is in the relevant range, it may be directly determined from the study of the IGW spectrum, as we have explained in the previous section. In such a case, we can determine one of the very important parameter, T_R . Thus, in this section, we consider the case where T_R is very high; even in such a case, we will see that we may have a chance to acquire the upper and lower bounds on T_R .

As we have discussed, the reheating temperature is as high as 10^{10} GeV if the inflaton decays via a Planck-suppressed operator. In such a case, the IGW spectrum at $f \sim 1 \text{ Hz}$ is

^{#10} In some panels of Fig. 13, one finds that analyses with $f_{\text{min}} = 0.3 \text{ Hz}$ give stronger constraints than those with $f_{\text{min}} = 0.1 \text{ Hz}$. This is an artifact of the prior region we choose. For the fiducial value of $T_R \simeq 10^{7.5} \text{ GeV}$ in the middle figures, for example, the upper bound is stronger for $f_{\text{min}} = 0.3 \text{ Hz}$ for BBO-grand and ult-DECIGO. If one tries to fit the fiducial GW spectrum with $T_R = 10^{7.5} \text{ GeV}$ using a postulated GW spectrum with postulated value of T_R higher than the fiducial T_R , the best-fit value of n_T is smaller (the absolute value is larger) for $f_{\text{min}} = 0.3 \text{ Hz}$, and therefore such a postulated value of T_R tends to be rejected for $f_{\text{min}} = 0.3 \text{ Hz}$. If n_T is fixed to the fiducial value (top figures), there is no such an artifact.

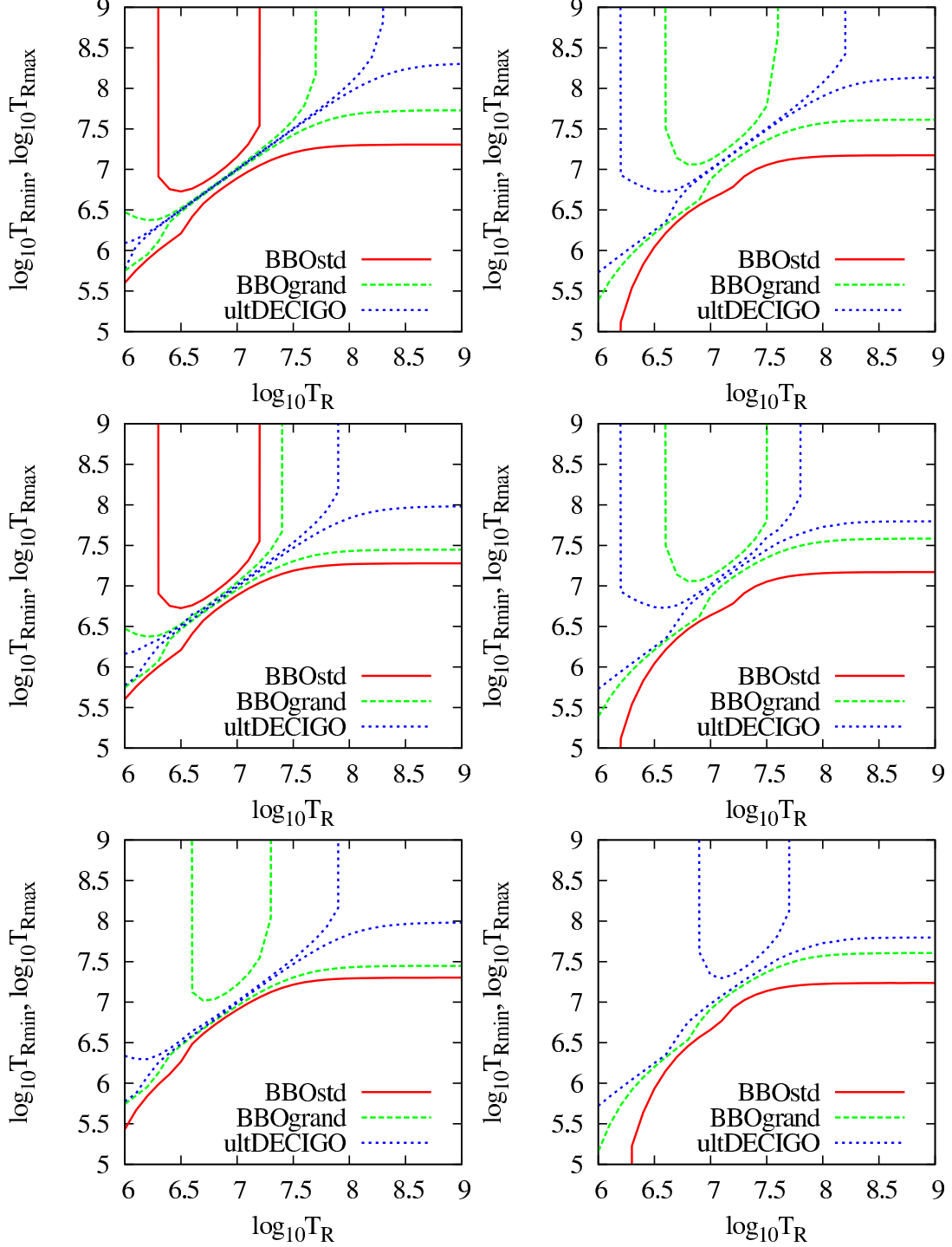


Figure 13: Upper and lower bounds on T_R obtained from BBO-std, BBO-grand and ult-DECIGO for $f_{\min} = 0.1$ Hz (left) and 0.3 Hz (right). In each figure, $\ln \bar{\Omega}_{\text{IGW}}$ is marginalized with a flat prior for $-\infty < \ln \bar{\Omega}_{\text{IGW}} < -15.3$. Also, n_T is fixed to the fiducial value (top), marginalized for $-0.1 < n_T < 0$ (middle) and marginalized for $n_T < 0$ (bottom).

insensitive to the reheating temperature, and hence the procedure to determine T_R discussed in the previous section is difficult. As shown in Table 1, however, $\bar{\Omega}_{\text{IGW}}$, n_T and α_T have slight dependences on the reheating temperature (if the value of m_ϕ is fixed). This is because the number of the e -folding during the inflation varies as the reheating temperature changes. Then, the inflaton amplitude at the time of the horizon exit of the mode f_* , which is denoted as ϕ_* , changes.

In the chaotic inflation model with the inflaton potential given in Eq. (2.14), the expansion rate and the slow-roll parameters at the time when the mode f_* exits the horizon are given by

$$H_* = \frac{m_\phi \phi_*}{\sqrt{6} M_{\text{Pl}}}, \quad \epsilon_* = \eta_* = 2 \frac{M_{\text{Pl}}^2}{\phi_*^2}. \quad (5.1)$$

Thus, combining these relations with Eqs. (2.9) and (2.10), the values of m_ϕ and ϕ_* may be obtained with the measurement of $\bar{\Omega}_{\text{IGW}}$ and n_T . Because the value of ϕ_* (and hence n_T) is insensitive to m_ϕ , information about n_T can be translated to that about the reheating temperature. As shown in Table 1, the predicted value of n_T varies from -0.0710 to -0.0581 for $T_R = 10^7 - 10^{12}$ GeV. Thus, the error in the measurement of n_T should be at the level of $O(10^{-3})$ in order to acquire sensible information about the reheating temperature. The noise level slightly better than that of BBO-grand is required in order to perform such an analysis. If the noise level of ult-DECIGO is available, on the contrary, n_T can be precisely determined. In such a case, assuming the chaotic inflation, T_R is well determined even if f_R is out of the sensitivity range of the GW detectors. For example, assuming that n_T is measured as $n_T = -0.0639 \pm 0.00061$ and $n_T = -0.0639 \pm 0.00093$, which are the expected accuracy in the two- and three-parameter analysis with $f_{\text{min}} = 0.1$ Hz, respectively (see Table 4), the reheating temperature is estimated to be $(0.6 - 1.5) \times 10^{10}$ GeV and $(0.5 - 1.9) \times 10^{10}$ GeV, respectively.

6 Conclusions and Discussion

We have discussed the prospects of the measurement of IGW spectrum using future space-based GW detectors, like BBO and DECIGO. We have performed a detailed analysis for the determination of IGW parameters, i.e., the amplitude $\bar{\Omega}_{\text{IGW}}$, the tensor spectral index n_T , and its running α_T . We have adopted the chaotic inflation model with parabolic inflaton potential as a fiducial model, and calculated the IGW amplitude for the frequency relevant for the IGW detectors. Then, using such an amplitude as well as tensor spectral index and running as the fiducial values, we performed a statistical analysis to estimate the expected accuracy of the measurements of these parameters. Here, we considered two cases. One is the case with high enough reheating temperature T_R , for which the IGW spectrum becomes insensitive to T_R . The other is the case where T_R is so low that the IGW detectors may directly observe the signal of the reheating; in such a case, the which is the IGW spectrum is significantly suppressed in high frequency region.

In the case with high enough reheating temperature, we have shown expected accuracies of the measurements of $\bar{\Omega}_{\text{IGW}}$, n_{T} , and α_{T} , adopting several noise parameters (which we call BBO-std, BBO-grand, and ult-DECIGO). Adopting the chaotic inflation model which predicts $r \sim 0.15$ at the CMB scale, we have seen that non-zero value of the tensor spectral index n_{T} may be confirmed with the noise level of BBO-grand with a few years of operation. For the detection of the running of the tensor mode, on the contrary, significant improvement of the noise level is necessary if $\alpha_{\text{T}} \sim O(10^{-3})$.

If the reheating temperature is relatively low, on the contrary, the future space-based GW detectors may put lower and upper bounds on T_{R} . We have seen that, if the fiducial value of the reheating temperature, \hat{T}_{R} , is $\sim 10^{6.5} - 10^{7.5}$ GeV, the reheating temperature can be well constrained. We have estimated the expected bounds on the reheating temperature. In particular, with the two-parameter analysis taking $\bar{\Omega}_{\text{IGW}}$ and T_{R} as free parameters, we have seen that the reheating temperature can be determined with the error of $\sim 30\%$ with BBO-std and $\sim 5\%$ with BBO-grand if $\hat{T}_{\text{R}} \sim 10^7$ GeV, assuming 10 years of operation and the minimum frequency $f_{\text{min}} = 0.1$ Hz. If $\hat{T}_{\text{R}} \gtrsim 10^8$ GeV, on the contrary, the reheating temperature is bounded only from below. We have also compared our results with full likelihood with those with Fisher matrix analysis. We have seen the results of two analysis may differ significantly in some cases.

The determination of the tensor-to-scalar ratio provides important information about the normalization of the cosmic IGW background. Although it may be premature to conclude that $r \sim O(0.1)$ based only on the result of BICEP2, our knowledge about the B -mode signal will be significantly improved in the near future because many efforts to detect the B -mode signal in CMB are on-going. Once the existence of the IGWs is confirmed by the observation of the B -mode signal in the near future, the program to detect and study the IGW spectrum in future space-based GW detectors is strongly suggested. Such a program will provide important and unique information about inflation.

Note Added

While we are finalizing this manuscript, the paper [34] appeared on the arXiv, which may have some overlap with our analysis.

Acknowledgements

The authors are grateful to M. Ando for valuable discussion. They appreciate useful comments by J. 'I. Yokoyama. They also thank A. Taruya for correspondence concerning their works. One of the authors (T.M.) is grateful to the Mainz Institute for Theoretical Physics (MITP) for its hospitality and its partial support during the completion of this work. This work is supported by JSPS KAKENHI Grant No. 26400239 (T.M.), No. 60322997 (T.M.), No. 23740195 (T.T.). R.J. is supported by the JSPS fellowship (No. 25-8360) and also by Program for Leading Graduate Schools, MEXT, Japan.

References

- [1] P. A. R. Ade *et al.* [BICEP2 Collaboration], arXiv:1403.3985 [astro-ph.CO].
- [2] A. D. Linde, Phys. Lett. B **129**, 177 (1983).
- [3] M. S. Turner, Phys. Rev. D **55**, 435 (1997) [astro-ph/9607066].
- [4] J. R. Pritchard and M. Kamionkowski, Annals Phys. **318**, 2 (2005) [astro-ph/0412581].
- [5] T. L. Smith, M. Kamionkowski and A. Cooray, Phys. Rev. D **73**, 023504 (2006) [astro-ph/0506422].
- [6] A. Cooray, Mod. Phys. Lett. A **20**, 2503 (2005) [astro-ph/0503118].
- [7] T. L. Smith, H. V. Peiris and A. Cooray, Phys. Rev. D **73**, 123503 (2006) [astro-ph/0602137].
- [8] S. Chongchitnan and G. Efstathiou, Phys. Rev. D **73**, 083511 (2006) [astro-ph/0602594].
- [9] B. C. Friedman, A. Cooray and A. Melchiorri, Phys. Rev. D **74**, 123509 (2006) [astro-ph/0610220].
- [10] T. L. Smith, M. Kamionkowski and A. Cooray, Phys. Rev. D **78**, 083525 (2008) [arXiv:0802.1530 [astro-ph]].
- [11] J. Caligiuri and A. Kosowsky, Phys. Rev. Lett. **112**, 191302 (2014) [arXiv:1403.5324 [astro-ph.CO]].
- [12] M. J. Mortonson and U. Seljak, arXiv:1405.5857 [astro-ph.CO].
- [13] R. Flauger, J. C. Hill and D. N. Spergel, arXiv:1405.7351 [astro-ph.CO].
- [14] N. Seto, Phys. Rev. D **73**, 063001 (2006) [gr-qc/0510067].
- [15] N. Seto and J. 'I. Yokoyama, J. Phys. Soc. Jap. **72**, 3082 (2003) [gr-qc/0305096].
- [16] K. Nakayama, S. Saito, Y. Suwa and J. 'i. Yokoyama, Phys. Rev. D **77**, 124001 (2008) [arXiv:0802.2452 [hep-ph]].
- [17] K. Nakayama, S. Saito, Y. Suwa and J. 'i. Yokoyama, JCAP **0806**, 020 (2008) [arXiv:0804.1827 [astro-ph]].
- [18] S. Kuroyanagi, C. Gordon, J. Silk and N. Sugiyama, Phys. Rev. D **81**, 083524 (2010) [Erratum-ibid. D **82**, 069901 (2010)] [arXiv:0912.3683 [astro-ph.CO]].
- [19] K. Nakayama and J. 'i. Yokoyama, JCAP **1001**, 010 (2010) [arXiv:0910.0715 [astro-ph.CO]].

- [20] S. Kuroyanagi, K. Nakayama and S. Saito, Phys. Rev. D **84**, 123513 (2011) [arXiv:1110.4169 [astro-ph.CO]].
- [21] S. Kuroyanagi, C. Ringeval and T. Takahashi, Phys. Rev. D **87**, 083502 (2013) [arXiv:1301.1778 [astro-ph.CO]].
- [22] G. M. Harry, P. Fritschel, D. A. Shaddock, W. Folkner and E. S. Phinney, Class. Quant. Grav. **23**, 4887 (2006) [Erratum-ibid. **23**, 7361 (2006)].
- [23] N. Seto, S. Kawamura and T. Nakamura, Phys. Rev. Lett. **87**, 221103 (2001) [astro-ph/0108011].
- [24] P. A. R. Ade *et al.* [Planck Collaboration], arXiv:1303.5076 [astro-ph.CO].
- [25] M. Tinto and S. V. Dhurandhar, Living Rev. Rel. **8**, 4 (2005) [gr-qc/0409034].
- [26] F. B. Estabrook, M. Tinto and J. W. Armstrong, Phys. Rev. D **62**, 042002 (2000).
- [27] V. Corbin and N. J. Cornish, Class. Quant. Grav. **23**, 2435 (2006) [gr-qc/0512039].
- [28] N. J. Cornish, Phys. Rev. D **65**, 022004 (2002) [gr-qc/0106058].
- [29] T. A. Prince, M. Tinto, S. L. Larson and J. W. Armstrong, Phys. Rev. D **66**, 122002 (2002) [gr-qc/0209039].
- [30] K. R. Nayak, A. Pai, S. V. Dhurandhar and J-Y. Vinet, Class. Quant. Grav. **20**, 1217 (2003) [gr-qc/0210014].
- [31] H. Kudoh, A. Taruya, T. Hiramatsu and Y. Himemoto, Phys. Rev. D **73**, 064006 (2006) [gr-qc/0511145].
- [32] R. Jinno, T. Moroi and K. Nakayama, Phys. Lett. B **713** 129, (2012) [arXiv:1112.0084 [hep-ph]].
- [33] R. Jinno, T. Moroi and K. Nakayama, JCAP **1401** 040, (2014) [arXiv:1307.3010].
- [34] S. Kuroyanagi, S. Tsujikawa, T. Chiba and N. Sugiyama, arXiv:1406.1369 [astro-ph.CO].